NACA

RESEARCH MEMORANDUM

JET EFFECTS ON BASE AND AFTERBODY PRESSURES OF A CYLINDRICAL AFTERBODY AT TRANSONIC SPEEDS

By James M. Cubbage, Jr.

Langley Aeronautical Laboratory
Langley Field, Va.

NATIONAL ADVISORY COMMITTEE
FOR AERONAUTICS

WASHINGTON
May 23, 1956
Declassified April 15, 1958

NATIONAL ADVISORY COMMITTEE FOR AERONAUTICS

RESEARCH MEMORANDUM

JET EFFECTS ON BASE AND AFTERBODY PRESSURES OF A CYLINDRICAL AFTERBODY AT TRANSONIC SPEEDS

By James M. Cubbage, Jr.

SUMMARY

An investigation has been conducted at transonic stream Mach numbers to study the effects of a cold jet issuing from the base of a cylindrical afterbody upon the afterbody and base pressures. Both sonic and supersonic conical nozzles were studied in this investigation with jet-to-base diameter ratios ranging from 0.25 to 0.85. Free-stream Mach numbers ranged from 0.6 to 1.25 and the jet total-pressure ratio from the no-jet flow condition to approximately 8.0. The effect on base pressure of introducing small quantities of air into the region adjacent to the base annulus was also investigated.

The results show that for the configuration tested the effect of the issuing jet on base pressure was, in general, detrimental at jet total-pressure ratios less than about 5.0 over the range of Mach numbers investigated. Very low base pressures were obtained at sonic free-stream velocities with a jet total-pressure ratio of about 2 to 3. The effect on base pressure of varying the jet-to-base diameter ratio was pronounced. Base bleed was beneficial in reducing the base drag under certain conditions and had little or no effect under other conditions.

INTRODUCTION

The range capabilities of supersonic aircraft may be substantially improved by cruising at the lower transonic speeds where less thrust is required. In order to realize maximum jet efficiency in this speed range, the size of the jet nozzle must be reduced from that required for the maximum supersonic speed of the aircraft. If this requirement of variable nozzle area is satisfied without changes in the afterbody contour, then the area of the annulus between the afterbody and nozzle exit must increase as the speed of the aircraft decreases. As a result of the decrease in the static pressure over the enlarged base annulus, a base drag of appreciable magnitude may be experienced.

Although a considerable volume of data is available to show the variations in magnitude of the base pressure as a function of nozzle and afterbody contour, of nozzle diameter relative to base diameter, and of jet pressure ratio in the supersonic region, relatively little has been done at transonic speeds. A recent comprehensive investigation of a series of contoured afterbodies for a range of boattail angles and jet-to-base diameter ratios at transonic Mach numbers up to 1.1 is reported in reference 1. Reference 2 contains similar data at high subsonic speeds. Data from other investigations are available but for the most part are restricted to tests of specific configurations in which the determination of base drag was a secondary objective.

The investigation reported herein was conducted in the Langley internal aerodynamics laboratory to determine the effect of jet total-pressure ratio, jet-to-base diameter ratio, and nozzle geometry on the base and afterbody pressures of a cylindrical afterbody at transonic stream Mach numbers. The jet-to-base diameter ratio was varied from 0.25 to 0.75 for the sonic nozzles and from 0.75 to 0.85 for the supersonic nozzles. Jet nozzle angles ranged from 0° to -25° for the conical sonic nozzles and from 5° to 25° for the supersonic conically convergent-divergent nozzles. The supersonic nozzles had an area expansion equivalent to a Mach number of 2.0. The effect on the base pressure of introducing small quantities of air into the dead air region adjacent to the base annulus was also investigated.

The present investigation covered a Mach number range from $M_\infty = 0.6$ to 1.25 with corresponding Reynolds numbers of 3.4×10^6 to 4.2×10^6 per foot. The jet total-pressure ratio H_j/p_∞ was varied from no jet flow to $H_j/p_\infty \approx 8$. The jet stagnation temperature for all tests reported herein was approximately 70° F.

SYMBOLS

A_b area of base annulus, $\frac{\pi}{4}\left(d_b^2 - d_j^2\right)$

A_{bl} area of annular base bleed opening

C_p pressure coefficient, $\dfrac{\frac{p}{p_\infty} - 1}{\frac{\gamma}{2} M_\infty^2}$

d diameter

H	total pressure
M	Mach number
M_c	Mach number corresponding to p_c/H_o
M_D	design Mach number of supersonic nozzle based on area ratio
p	static pressure
s	distance upstream along afterbody from plane of afterbody base
u	velocity of flow at distance y from model support tube and parallel to tunnel center line
U_∞	free-stream velocity
x	distance along center line of test section from upstream end of slot (slot origin)
y	perpendicular distance from model support tube
δ	boundary-layer thickness
θ	nozzle half-angle; positive when diverging in the direction of flow from center line of nozzle
γ	ratio of specific heats

Subscripts:

a	afterbody
b	base
c	plenum chamber surrounding test section
j	jet
o	stagnation conditions
∞	free stream

APPARATUS

Tunnel

The $8\frac{1}{2}$- by 12-inch slotted test section employed in this investigation is shown in the photograph of figure 1(a) and in the drawing of figure 1(b). Each of the top and bottom walls contained four slots; the width of the slots was such that the open-to-closed area ratio of the slotted wall was 1/8. The individual slots were tapered in both width and depth over the first 7 inches of their length; the width increased from 0 to 3/8 inch, while the depth decreased from 1 to 1/8 inch. From $x = 7$ to the end of the slot, the slot cross section remained constant.

The stream-tube expansion necessary to accelerate the flow to supersonic velocities was accomplished by removal of air through the slots into the interconnected chambers outside the slotted walls. At low supersonic velocities, this air was returned to the main stream at the downstream end of the slotted section where the cross-sectional area of the passage was approximately 16 percent larger than the geometric minimum at the upstream end of the tunnel. Auxiliary suction was used to extend the Mach number range of the tunnel from 1.18 to 1.25 and to maintain a constant Mach number in the test section as the jet total-pressure ratio was varied. Air for the tunnel main stream was supplied by two centrifugal blowers through a 40-inch-diameter supply duct. The maximum tunnel stagnation pressure available for these tests was approximately $1\frac{3}{8}$ atmospheres at a stagnation temperature of 180° F.

The model support consisted of a 2-inch-diameter tube cantilevered from the tunnel entrance bell as shown in figures 1(b) and 2. The upstream support struts were hollow, the two lower struts containing all pressure leads while the top strut was used to duct high-pressure air to the model support tube. The downstream struts were solid and of hexagonal cross section. The jet air was supplied from three 1,000-cubic-foot tanks which were pressurized to approximately 100 pounds per square inch. Pneumatically operated valves were used to maintain a constant pressure at the entrance of the jet nozzle.

Models

A total of 16 jet nozzles were studied in this investigation. Drawings of these models and photographs of several models are presented as figure 3. The original four sonic-nozzle models had convergent angles θ of 0°, -5°, -12°, and -25° and a jet exit diameter equal to 65 percent of the base diameter $\left(d_j/d_b = 0.65\right)$. The 0° and -12°

nozzles were later modified to $d_j/d_b = 0.75$. Limited data were also taken for a $\theta = -25^\circ$ nozzle with $d_j/d_b = 0.25$ and 0.45. The initial three supersonic nozzles had divergence angles of 5°, 12°, and 25° with $d_j/d_b = 0.75$. The diameter ratio for the 12° model was later increased to 0.85. The convergence angle and throat length as well as the ratio of throat area to jet exit area ($M_D = 2.0$) were identical for all of the supersonic models investigated.

Four base-bleed models (figs. 3(c) and 3(d)) utilized the jet supply air as a source for the bleed flow. Reductions in the base-bleed flow rate at a particular jet pressure ratio were accomplished by closing off a number of the bleed-flow throttling orifices. For the tests reported herein, data were taken with 16, 8, and 4 throttling orifices open. The exit area for the bleed flow on the 0° nozzle was increased by removing the thin flange at the end of the model. A baffle ring was installed as shown in figure 3(c) to throttle the high-velocity flow issuing from the bleed-flow orifices.

A boundary-layer survey model, shown in place in the tunnel in figure 4, was used to estimate the thickness of the boundary layer on the support tube at a station $5\frac{1}{2}$ inches upstream of the base of the afterbody. The two survey rakes were located on the vertical center line of the tunnel and each was composed of five 0.040-inch-diameter total-pressure tubes spaced 0.01, 0.025, 0.04, 0.1, and 0.25 inch from the surface of the model support tube.

Instrumentation

The stream stagnation pressure and temperature were measured in the upstream 40-inch-diameter supply duct while the test-section reference static pressure p_c was measured in the tunnel plenum chamber. Static-pressure orifices along the center line of one side wall were used to obtain tunnel Mach number distributions; for these tests, a metal plate with orifices spaced at 1-inch intervals replaced one window.

Along the model afterbody, static-pressure orifices were installed on two meridians 180° apart; the axial location of these orifices is shown in figure 3(a). Base pressure was measured by a single orifice located 0.055 inch from the outer edge of the base as shown in figure 3(a). The 0.040-inch-diameter total-pressure probe shown in figure 4 was used to obtain jet total-pressure profiles across the vertical diameter of the jet exit. The end of the probe passed within 1/64 inch of the base of the model (except in the case of the boundary-layer survey model) and the pressure was continuously recorded by two 2-variable recording potentiometers.

All static pressures, with the exception of the two in the throat of the jet-flow metering venturi, were recorded photographically from multitube manometer boards containing tetrabromoethane. The venturi static pressures and the total pressure in the entrance tube were recorded visually from mercury-filled U-tube manometers at low pressures and from Bourdon gages at the higher pressures. The tunnel stagnation pressure was read from a mercury-filled U-tube manometer.

RESULTS AND DISCUSSION

Tunnel Mach Number Distributions and Wall Interference Effects

Time-averaged Mach number distributions determined from the tunnel stagnation pressure H_o and static pressures along the center line of one side wall of the tunnel are presented in figure 5. The corresponding values of M_c, as computed from the chamber static pressure p_c and the tunnel stagnation pressure, are shown on the left-hand side of the figure.

The effect of the presence of the model and support tube on the Mach number distributions is shown in figure 5(a) where distributions for the empty tunnel are compared with those obtained when the model was in place. Figure 5(b) compares distributions for the case of no jet flow with those for the case of a sonic nozzle operating at a jet total-pressure ratio of about 4.0. The expansion of the tunnel flow at the jet exit station at values of $M_\infty \geq 1.0$ is noted in the comparison of figure 5(a). The distribution for $M_\infty = 1.0$ shows an expansion originating a short distance upstream of the jet exit station. Since this expansion would probably be reflected from the wall as a further expansion, the measured base pressure for this speed may be excessively low. At $M_\infty > 1.0$ the expansion of the stream is propagated essentially along characteristic lines and reaches the wall at an increasing distance from the jet exit station as M_∞ increases. Thus, the reflected disturbance would influence pressures only at points downstream of the jet exit station. In reference 3, strong shock waves intersecting the wake of blunt bases 3 diameters downstream of the base were shown to influence base pressure; hence, for the case of no jet flow, some effect of wall-reflected disturbance may be present at the lower supersonic speeds. For the jet-on case, except when the reflected disturbance intersects the subsonic flow near the base between the external and jet flow, no error would be expected since disturbances could not be propagated upstream through the surrounding supersonic flow. The effect of the jet on the distributions can be seen in figure 5(b) as a change in the distributions downstream of the jet exit station due to the reduced expansion at the afterbody base.

At speeds less than sonic, the time-averaged Mach number distributions of figure 5 do not show any abrupt variations. This result would indicate that any disturbance present is of a transient nature. The gradual deviation of the distribution for $M_\infty = 0.9$ (fig. 5(a)), is thought to be due in part to the boundary layer on the model support tube and the increased sensitivity of the flow to small changes in area near sonic speeds and to the acceleration of the flow as it turns towards the center line of the tunnel to compensate for the increased cross-sectional area downstream of the model.

Although the areas of probable interference effects are discernible, the magnitude of these effects on the data to be presented is undetermined. Therefore, no corrections for tunnel-wall-interference effects have been applied to the data.

Afterbody Boundary Layer

The boundary-layer velocity distribution on the model support tube as measured at a point $5\frac{1}{2}$ inches upstream of the afterbody base at several stream Mach numbers is shown in figure 6(a). A comparison of the boundary-layer profile at $M_\infty = 0.9$ with a 1/7-power profile in figure 6(b) shows that the boundary layer in these tests was fully turbulent. The data points in these figures represent an average between the data recorded from the two boundary-layer survey rakes. It may be seen in figure 6(a) that from the fairing used the thickness of the boundary layer on the afterbody was approximately 20 percent of the base diameter. This is somewhat larger than what would normally be found on a conventional aircraft configuration. The data of reference 4 show that, for a cylindrical afterbody at a free-stream Mach number of about 2.0, the base pressure coefficient was not significantly affected by increasing δ/d_b from 0.05 to 0.18.

Base Pressure

Effect of jet total-pressure ratio.- Pressures measured on the base of the cylindrical afterbody with the several sonic nozzles of this investigation are presented in coefficient form in figure 7 as a function of jet total-pressure ratio for constant values of stream Mach number. Data similar to those of figure 7 are presented in figure 8 for the supersonic nozzles investigated. The variation of the base pressure with jet total-pressure ratio falls into one of two typical patterns dependent upon the stream Mach number. These patterns are shown in figure 9 with schlieren photographs of the flow field at specific points on the curves. The supersonic variation is shown in figure 9(a) while the subsonic one is shown in figure 9(b). The survey probe seen in the

schlieren photographs is located on the center line of the jet except in two instances (fig. 9(a)) where it is located approximately 2 inches directly above the jet center line. Consequently, the shock pattern within the jet is disturbed by the presence of the probe.

At $M_\infty = 1.2$ (fig. 9(a)) point (a) is the no-jet-flow condition where the external stream aspirates the base to a pressure lower than the stream static pressure through turbulent mixing along the wake boundary. The expansion of the tunnel flow at the base of the afterbody for this condition appears as a broad dark band in the corresponding schlieren photograph. As air from the nozzle enters the wake at very low flow rates, the base pressure coefficient increases because this additional mass exceeds the amount that can be removed by the mixing action along the wake boundary. At higher jet-flow rates, the higher velocity jet supplements the main-stream flow in aspirating the base to much lower pressures (point (b)). As the jet pressure ratio increases above that required for choking of the nozzle, near $H_j/p_\infty = 2$, the jet "blossoms" outward and the pressure rise through the trailing shock, produced by turning of the main-stream flow away from the jet axis by the jet, becomes of sufficient magnitude to increase the base pressure. The jet blossoms out further as H_j/p_∞ increases until at $H_j/p_\infty = 8$ the pressure rise through the strong trailing shock is sufficient to increase the base pressure above its value for the no-jet-flow condition. The increased strength of the trailing shock at the higher values of H_j/p_∞ is noted in the schlieren photographs as an increase in its inclination relative to the jet axis.

At $M_\infty = 0.9$ (fig. 9(b)) the variation of base pressure coefficient with jet total-pressure ratio differs somewhat from the pattern at supersonic stream Mach numbers. Up to $H_j/p_\infty \approx 1.5$, the variation of C_{p_b} is similar to that which occurred at $M_\infty \gtrsim 1.0$ (fig. 9(a)), but at this point the base pressure begins to increase until at $H_j/p_\infty \approx 2.0$ the curve again assumes a positive slope. This reflex in the curve is believed to be associated with choking of the jet nozzle and was observed for all models at subsonic speeds. At $H_j/p_\infty \approx 4$, the curve breaks and the base pressure again increases. At this pressure ratio the jet boundary has expanded outward enough so that the pressure rise connected with turning of the main stream away from the jet axis begins to be felt at the base. At $H_j/p_\infty = 6$, the jet boundary has expanded outward still further and consequently the turning of the main-stream flow occurs nearer the base and the resulting pressure rise has a stronger effect on the base pressure. The compression disturbances visible in the photograph for point (a) of figure 9(b) indicate shock waves in the local supersonic flow at the base of the afterbody and

acoustical compression waves which, originating in the wake and in the tunnel, are propagated forward. The latter disturbances are transient and do not appear in the time-averaged pressure distributions along the wall or model.

The base-pressure variation discussed above has been observed by others at higher supersonic Mach numbers where considerable research has been conducted on afterbody drag. The transonic picture of the flow is relatively new but it is observed here that the flow phenomena remain essentially the same.

The slope of the curves in figures 7(a) and (b) is shown to be nearly independent of nozzle angle for the sonic nozzles. For the supersonic nozzles (fig. 8) the slope of the curves, as well as the magnitude of C_{p_b}, varies with change in nozzle angle. Varying the jet size of the sonic nozzles effected substantial changes in the variation of base pressure coefficient with jet pressure ratio (fig. 7(c)).

Effect of stream Mach number.- The variation of base pressure coefficient with Mach number for a sonic and a supersonic nozzle at several jet pressure ratios is presented in figure 10. The supersonic data between $M_\infty = 1.6$ and 2.4 were obtained from reference 5. It will be noted that in figure 10(b) data for an $M_D = 2.5$ nozzle (ref. 5) are compared with the present data for an $M_D = 2.0$ nozzle. Other data of reference 5 show that within this range and at these jet static-pressure ratios the design Mach number for the conical convergent-divergent nozzles did not have a significant effect on the base pressure coefficient. Therefore, the difference in M_D for the two nozzles of this figure would have only a small effect on the curves. Figure 10 illustrates the rapid decrease in base pressure coefficient near sonic velocities and the magnitude of this coefficient with respect to that which occurs at higher supersonic speeds and at subsonic speeds. In addition, for the sonic nozzle, the difference in C_{p_b} for different values of jet pressure ratio is shown to increase substantially as M_∞ decreases.

A detailed presentation of base pressure coefficient as a function of Mach number is made in figure 11. These curves were obtained by cross-plotting the data of figures 7 and 8 at constant jet pressure ratios. The base pressure for the no-jet-flow condition is also indicated on each diagram to facilitate separation of the jet effects. For sonic nozzles, the variation in base pressure coefficient with Mach number is relatively small below $M_\infty \approx 0.9$. At $M_\infty > 0.9$ the effect of stream Mach number depends greatly on the jet pressure ratio. The effect of the jet was most adverse under conditions encountered in current turbojet cruise operation, $H_j/p_\infty \approx 4$ or less. The transonic drag rise at these pressure ratios was very large, indicating substantial penalties at $M_\infty > 0.9$.

At these jet pressure ratios, and on the basis of jet total pressure H_j the adverse effects of the jet on the base pressure were generally greater for nozzles designed for $M = 2$ than for sonic nozzles. For supersonic nozzles, the divergence rate is shown to exert a strong influence on the base pressure variation with Mach number and upon the level of the base pressures, whereas for sonic nozzles the effect of convergence angle was relatively small.

Effect of nozzle angle.- The base pressure coefficient is presented as a function of nozzle angle θ for constant values of jet-to-base diameter ratio in figure 12. Relatively little change occurred in C_{p_b} for the sonic nozzles (negative values of θ) at $H_j/p_\infty \leq 4$ over the range of nozzle angles investigated. At the higher jet pressure ratios ($H_j/p_\infty = 6$ and 8) the variation in C_{p_b} for the sonic nozzles became, in some instances, more pronounced. At $M_\infty = 1.0$ and $H_j/p_\infty = 8$ (fig. 12(c)), for example, the base pressure coefficient ranged from -0.045 at $\theta = -5^\circ$ to -0.165 at $\theta = -25^\circ$. This variation of base pressure with nozzle angle is thought to be due to the behavior of the boundary layer along the nozzle wall close to the exit of the nozzle, which results in an effective jet-to-base diameter ratio somewhat smaller than the geometric ratio. A reduction in d_j/d_b would delay the intersection of the jet and main-stream flow a corresponding amount and thus tend to decrease the base pressure at a given pressure ratio and Mach number of the free stream. The decrease in base pressure noted as θ decreased from -5° to 0° is thought to result from insufficient length of the constant-diameter throat of the 0° nozzle (the 0° nozzle was identical to the -5° nozzle except for the constant-diameter portion, as shown in fig. 3(c)). If the flow in the nozzle did not follow the contour of the nozzle, the jet flow would issue from the nozzle with a smaller diameter than the diameter of the jet exit and thus produce the effect mentioned previously.

For the supersonic nozzles, the variation of C_{p_b} with nozzle divergence angle was substantial. At low jet pressure ratios (below about 4.0), this variation in base pressure can be attributed largely to separation of the nozzle flow from the nozzle wall. This separation would reduce the diameter of the high-velocity portion of the jet and thus produce an effective jet-to-base diameter ratio less than the geometric one. Counteracting this effect to lower the base pressure is the effect of greater angularity of the jet flow with the external flow at large values of θ, which brings the intersection of the two flows closer to the base and thus tends to increase the base pressure. The extremely low base pressures measured at $M_\infty = 1.0$ (fig. 12(c)) for the supersonic nozzles may reflect significant tunnel interference at this speed.

The sonic and supersonic nozzles may be compared on the basis of jet static-pressure ratio in figures 12(c), (d), and (e) since this ratio is approximately equal to 1 for the sonic nozzle at $H_j/p_\infty = 2$ and for the supersonic nozzle at $H_j/p_\infty = 8$. On this basis, the supersonic nozzles have a greater base pressure than the sonic nozzles. The resulting curve is approximately continuous from $\theta = -25^\circ$ to $\theta = 25^\circ$ except at $M_\infty = 1.0$ where tunnel interference may be significant.

Effect of jet-to-base diameter ratio.- Figure 13 presents C_{p_b} as a function of jet-to-base diameter ratio for several values of H_j/p_∞ at $M_\infty = 0.9$ and 1.1. These curves were obtained by cross-plotting the data presented in figure 7 and, therefore, represent data from $\theta = 0^\circ$ and -25° nozzles. Since the effect of θ on C_{p_b} was relatively small for the sonic nozzles, except at the highest values of H_j/p_∞ as pointed out in the previous section, it is felt that the introduction of θ as a variable in figure 13 does not seriously affect the trend of the curves. Two points taken from the data of reference 2 are shown in figure 13(a). These points, which represent the base pressure coefficient obtained on cylindrical afterbody with $d_j/d_b = 0.375$ at $H_j/p_\infty = 2.29$ and 7.26, are consistent with the present data.

At small values of the jet-to-base diameter ratio, the jet and wake boundaries in the vicinity of the base are well separated, and increasing the jet diameter in the absence of interference between the jet and external stream decreases the base pressure coefficient. At the higher values of d_j/d_b, the effects of the jet on the external flow increase with jet-to-base diameter ratio and the value of C_{p_b} increases with increasing d_j/d_b. It is apparent that for some intermediate value of d_j/d_b the adverse pumping effects and the favorable interference effects will be compensating; at this value, the base pressure coefficient reaches a minimum. From figure 13, it can be seen that the jet pressure ratio corresponding to minimum base pressure increases as the jet-to-base diameter ratio decreases. At $M_\infty = 0.9$ (fig. 13(a)) the mimimum value of base pressure decreases as d_j/d_b decreases and H_j/p_∞ increases, while at $M_\infty = 1.1$ (fig. 13(b)) the minimum base pressure is nearly independent of d_j/d_b and H_j/p_∞.

Effect of base bleed.- In references 2, 6, and 7, a reduction in base drag was obtained by introducing small quantities of air into the region adjacent to the base annulus. Similar tests were made during the present investigation where air directed from the primary jet flow ahead of the nozzle was introduced into the base annulus through an annular

opening (fig. 3(c)). The bleed mass-flow rate, therefore, increased as the jet mass-flow rate increased. Calculations based upon the base pressure and the pressure in the small chamber upstream of the base bleed opening of the basic bleed model indicated that the maximum bleed mass-flow rate obtained was of the order of 2 to 3 percent of the jet mass-flow rate. Total-pressure surveys across the base annulus showed that the bleed flow issuing from the small annular opening on the basic bleed model with all throttling orifices open had considerable velocity at $H_j/p_\infty = 4$. This condition was detrimental to the base pressure in that the high-velocity bleed flow aided the jet flow in aspirating the base. By closing part of the throttling orifices, the mass-flow rate and velocity of the bleed flow were reduced approximately 75 percent. In order to reduce further the velocity of the bleed flow without changing the maximum bleed flow rate, the basic bleed model was modified to increase the exit area for the bleed flow from $0.06A_b$ to $0.18A_b$.

The maximum effect of base bleed on the base pressure of the nozzle with $\theta = 0^\circ$ and $d_j/d_b = 0.65$ when $A_{bl}/A_b = 0.06$ and 0.018 is shown in figure 14(a). For the basic bleed model this condition occurred with four throttling orifices open, and for the modified bleed model with all orifices open. It will be noted in figure 14(a) that base bleed caused a substantial increase in base pressure coefficient at certain conditions - for example, at $M_\infty = 1.0$ and $H_j/p_\infty = 2$ - while at a few other points there was little or no increase in base pressure. For the example cited, the base pressure coefficient increased by about 35 percent; however, even with this drag reduction, the base pressure was still quite low. In addition, the penalties incurred in obtaining the bleed flow may offset any drag reduction gained from increased base pressure. Data obtained for the basic bleed model with $\theta = -12^\circ$ are not shown since they were practically identical to the data for the model with $\theta = 0^\circ$.

Figure 14(b) presents the data obtained from the $\theta = 12^\circ$ supersonic nozzle with base bleed. This nozzle was not modified to the larger bleed-flow exit. As with the sonic nozzle, the greatest increase in base pressure coefficient occurred with only four throttling orifices open and only these data are presented. Substantial decrease in base pressure occurred for $H_j/p_\infty = 4$ and 6 below $M_\infty \approx 0.9$ and some increase occurred at $M_\infty > 1.10$.

Afterbody Pressure Distributions

Since the afterbody utilized in this investigation was cylindrical, the pressure drag of the afterbody is zero. Nevertheless, the pressures along the afterbody are of interest. Low pressures at the base lead to substantial reductions in pressure near the base (fig. 15). The distance

upstream from the base over which the afterbody pressure is influenced by proximity to the base decreases as M_∞ increases. In figure 15(a), for example, at $M_\infty = 0.6$, the afterbody pressure begins to decrease near $s/d_b = 1.0$ whereas at $M_\infty = 1.24$ the afterbody pressure is essentially constant to $s/d_b = 0.3$. The distance upstream from the base over which the base pressure would influence the static pressure on the afterbody would depend upon the thickness of the boundary layer on the afterbody and upon the local velocity within the boundary layer. At constant jet pressure ratio, decreasing the boundary-layer thickness or increasing the free-stream velocity would reduce this distance.

SUMMARY OF RESULTS

An experimental investigation at transonic speeds of jet effects on the flow over a cylindrical afterbody yielded the following results:

1. The influence of the jet upon the base static pressure was generally detrimental at jet total-pressure ratios equal to or less than 5.0 for the jet-to-base diameter ratios of about 0.75.

2. The jet total-pressure ratio at which the jet effects on base pressure became favorable decreased with increasing jet-to-base diameter ratio.

3. With sonic nozzles, the base pressure coefficient reached a minimum value of about -0.55 at a Mach number of 1 or greater; with supersonic nozzles, base pressure coefficients as low as -0.8 were measured. At subsonic speeds, the mimimum base pressure coefficient measured was about -0.3.

4. The convergence angle of the sonic nozzles investigated did not significantly affect the base or afterbody static pressures.

5. The divergence angle of the convergent-divergent nozzles affected the base pressure; for identical operating conditions ($M_\infty = 1.0$ and $H_j/p_\infty = 8.0$), the base pressure coefficient increased 49 percent as the divergence angle increased from 10° to 50°.

6. Base bleed was beneficial in reducing the base drag under certain conditions and had little or no effect under other conditions.

Langley Aeronautical Laboratory,
National Advisory Committee for Aeronautics,
Langley Field, Va., March 6, 1956.

REFERENCES

1. Henry, Beverly Z., Jr., and Cahn, Maurice S.: Preliminary Results of an Investigation at Transonic Speeds to Determine the Effects of a Heated Propulsive Jet on the Drag Characteristics of a Related Series of Afterbodies. NACA RM L55A24a, 1955.

2. Salmi, Reino J.: Experimental Investigation of Drag of Afterbodies With Exiting Jet at High Subsonic Mach Numbers. NACA RM E54I13, 1954.

3. Faro, I. D. V.: Experimental Determination of Base Pressures at Supersonic Velocities. Bumblebee Rep. No. 106, The Johns Hopkins Univ. Applied Physics Lab., Nov. 1949.

4. Cortright, Edgar M., Jr., and Kochendorfer, Fred D.: Jet Effects on Flow Over Afterbodies in Supersonic Stream. NACA RM E53H25, 1953.

5. Bromm, August F., Jr., and O'Donnell, Robert M.: Investigation at Supersonic Speeds of the Effect of Jet Mach Number and Divergence Angle of the Nozzle Upon the Pressure of the Base Annulus of a Body of Revolution. NACA RM L54I16, 1954.

6. Cortright, Edgar M., Jr., and Schroeder, Albert H.: Investigation at Mach Number 1.91 of Side and Base Pressure Distributions Over Conical Boattails Without and With Jet Flow Issuing From Base. NACA RM E51F26, 1951.

7. Cortright, Edgar M., Jr., and Schroeder, Albert H.: Preliminary Investigation of Effectiveness of Base Bleed in Reducing Drag of Blunt-Base Bodies in Supersonic Stream. NACA RM E51A26, 1951.

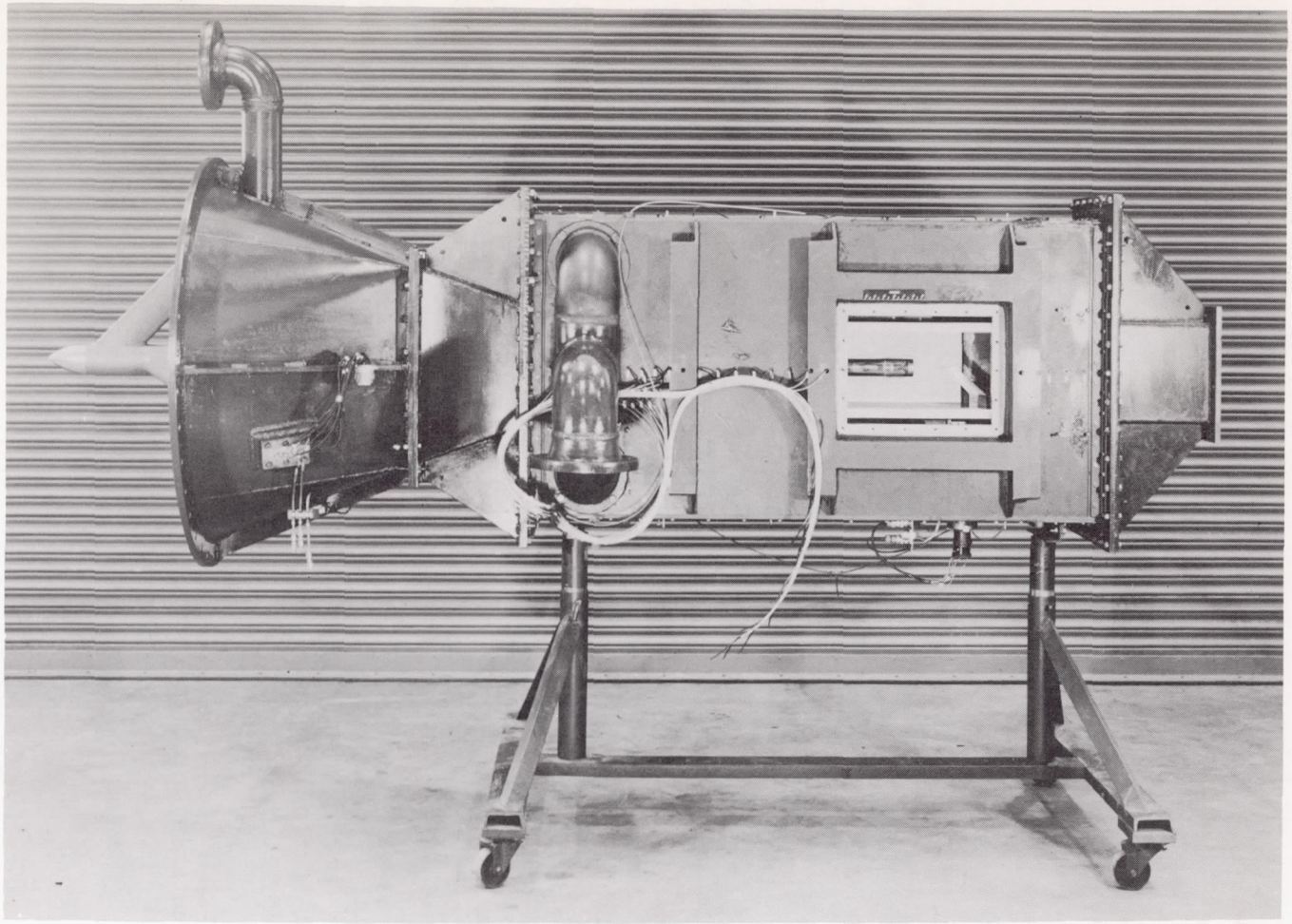

(a) $8\frac{1}{2}$ - by 12-inch slotted test section. L-84776

Figure 1.- Tunnel and model installation.

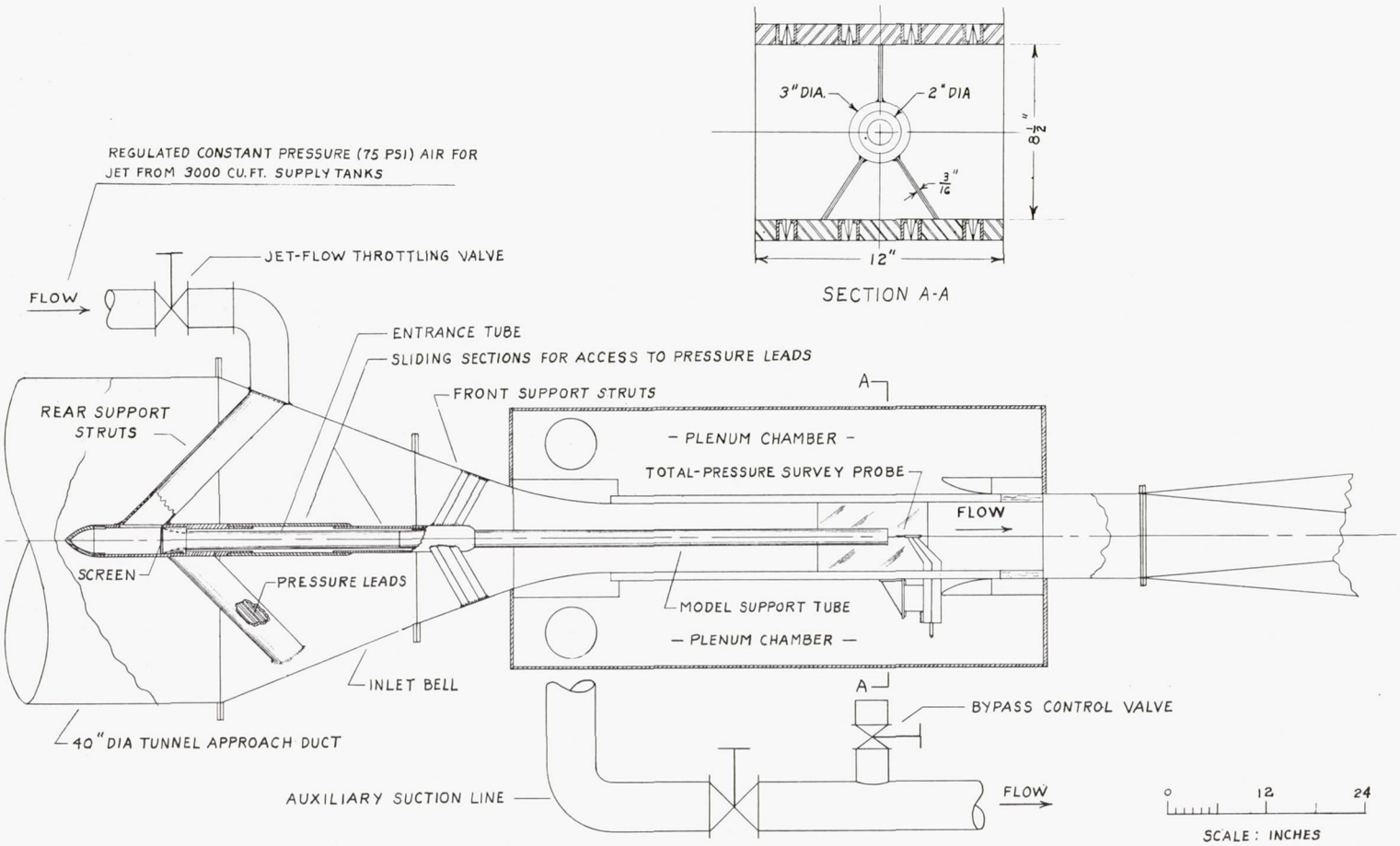

(b) Sketch of tunnel showing model installation.

Figure 1.- Concluded.

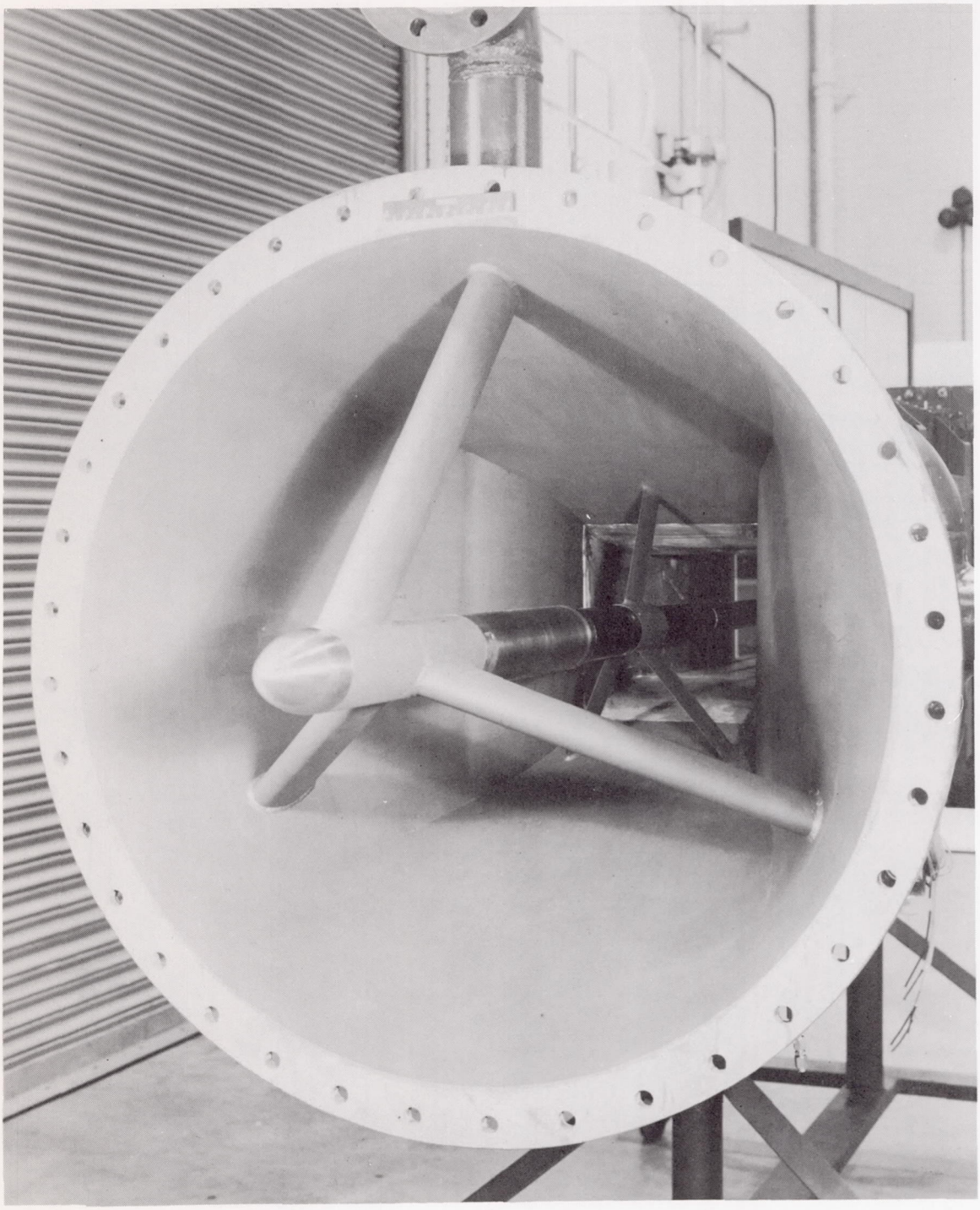

L-84775

Figure 2.- Tunnel inlet bell and support-strut arrangement.

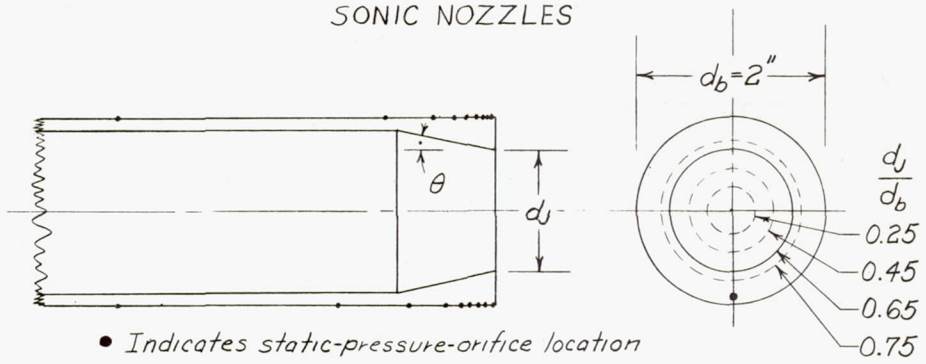

θ / d_j/d_b	0	-5°	-12°	-25°
0.25				X
0.45				X
0.65	X	X	X	X
0.75	X		X	

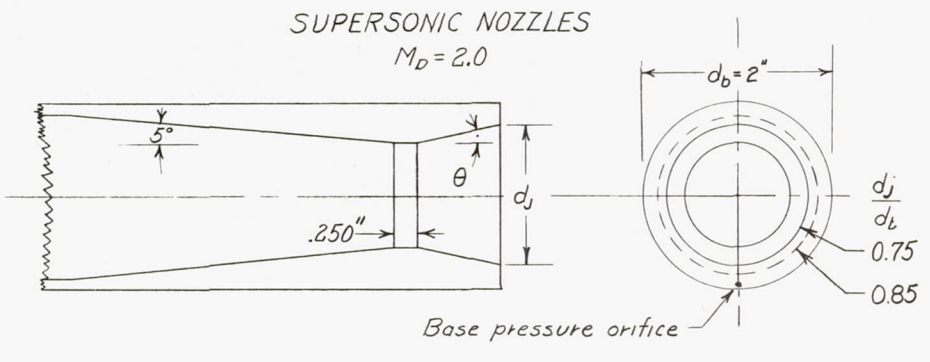

θ / d_j/d_b	5°	12°	25°
0.75	X	X	X
0.85		X	

(a) Basic jet-nozzle configurations.

Figure 3.- Jet-nozzle configurations.

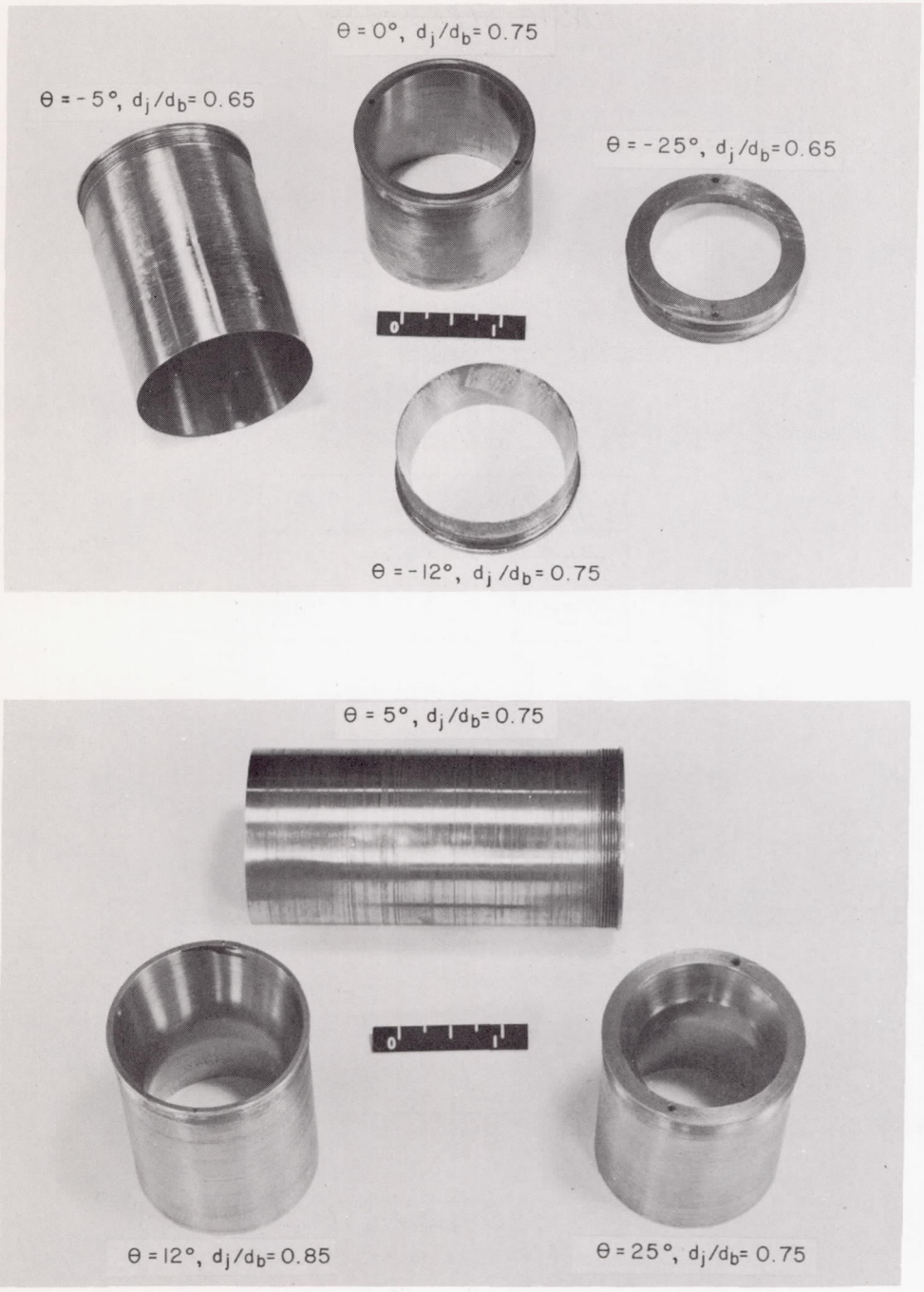

L-92445

(b) Photograph of several nozzle configurations.

Figure 3.- Continued.

BASIC BLEED MODELS

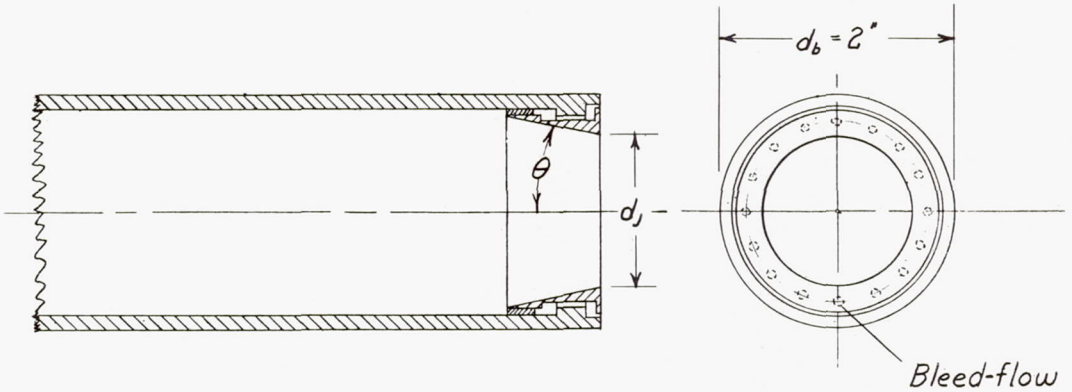

d_j/d_b \ θ	-12°	0°	12°
0.65	X	X	
0.75			X

MODIFIED BLEED MODEL

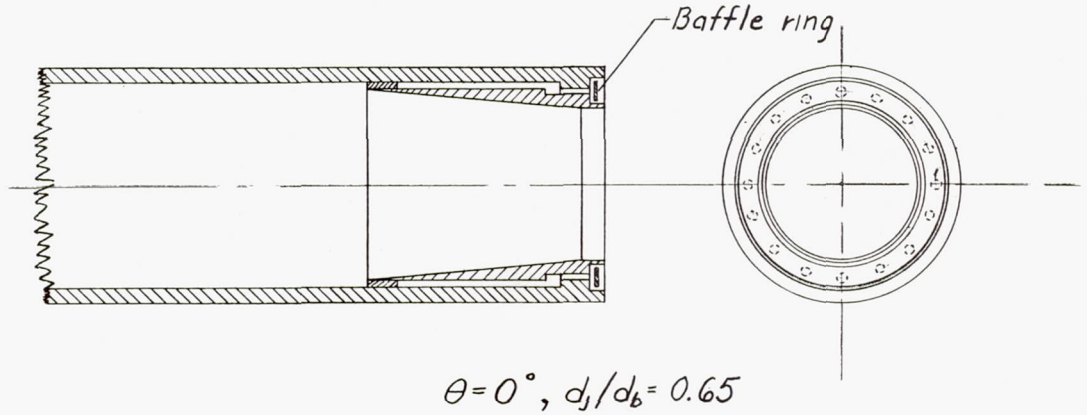

$\theta = 0°$, $d_j/d_b = 0.65$

(c) Base bleed configurations.

Figure 3.- Continued.

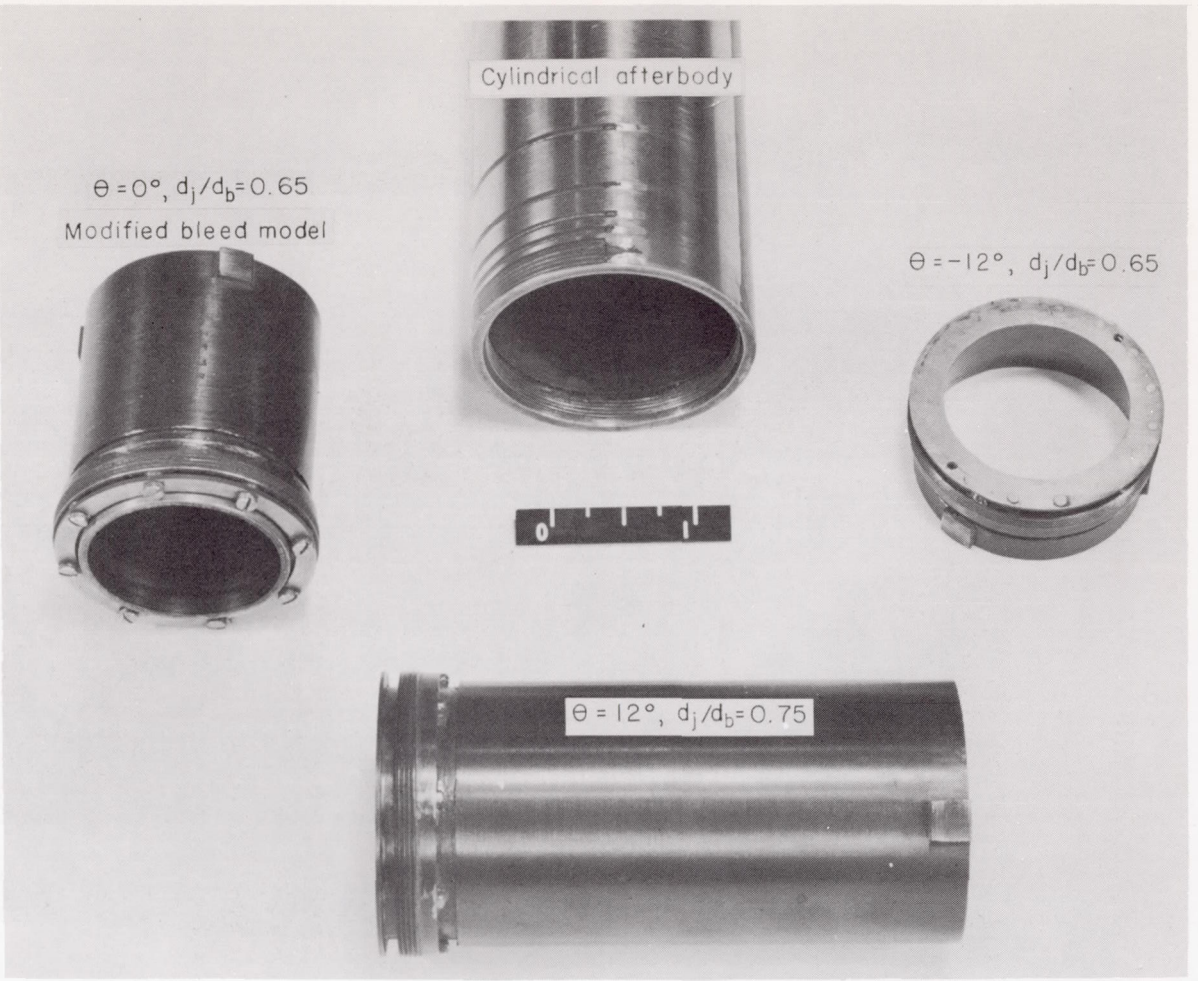

L-88597.1

(d) Base-bleed models and cylindrical afterbody.

Figure 3.- Concluded.

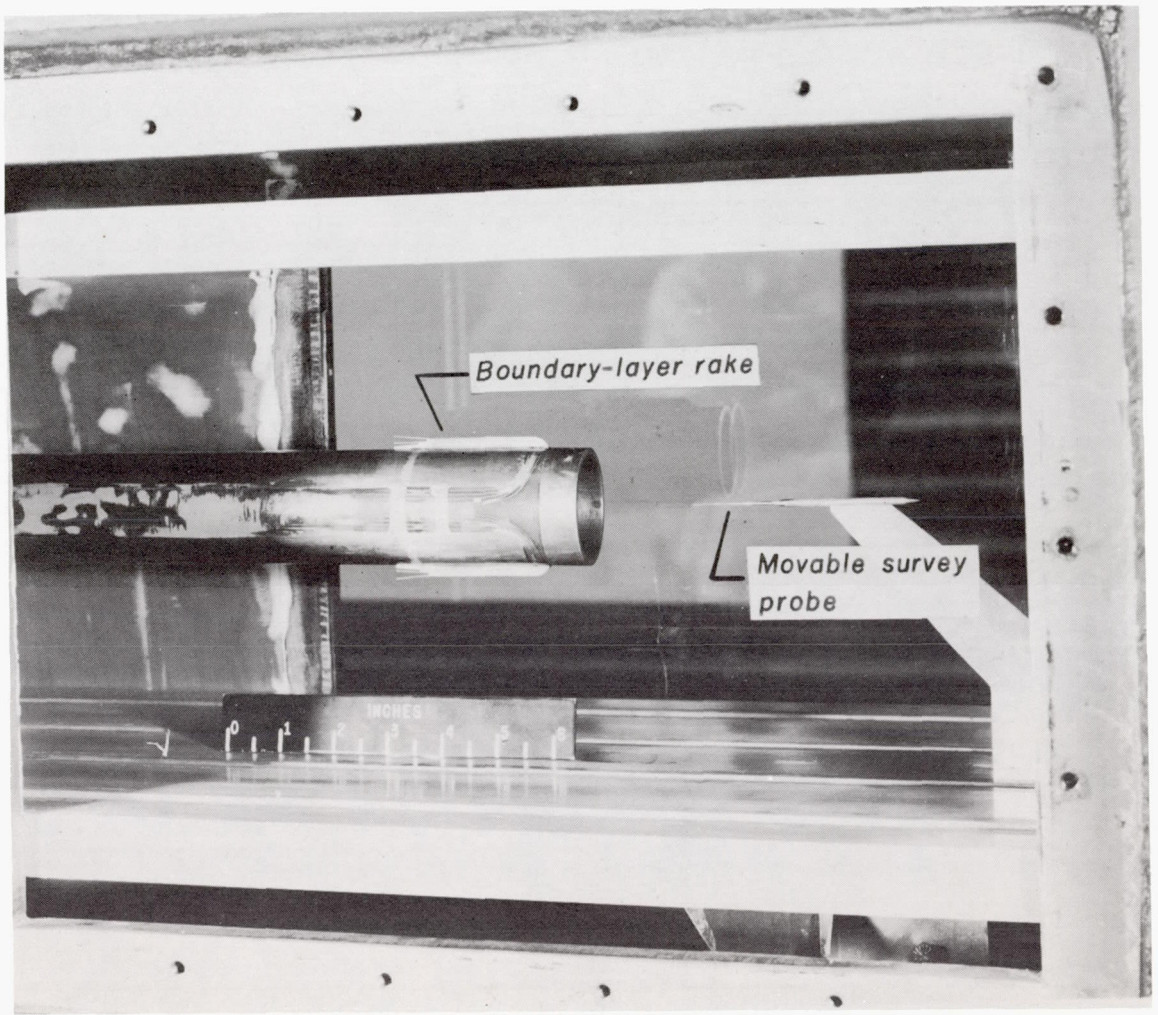

L-84777.1

Figure 4.- Boundary-layer model installed in tunnel.

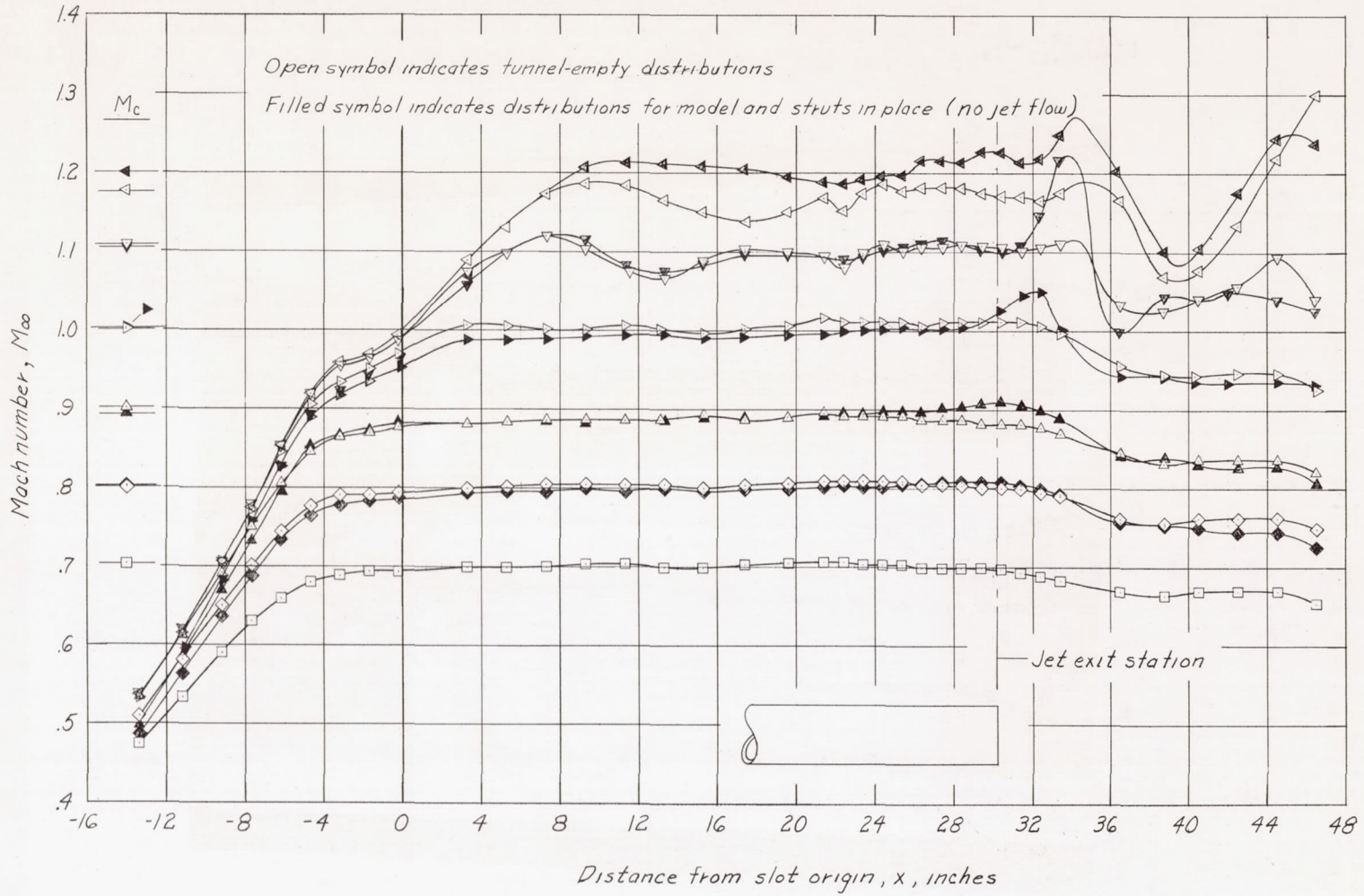

(a) Distributions for empty tunnel and for tunnel with model in place.

Figure 5.- Mach number distribution along solid wall of tunnel.

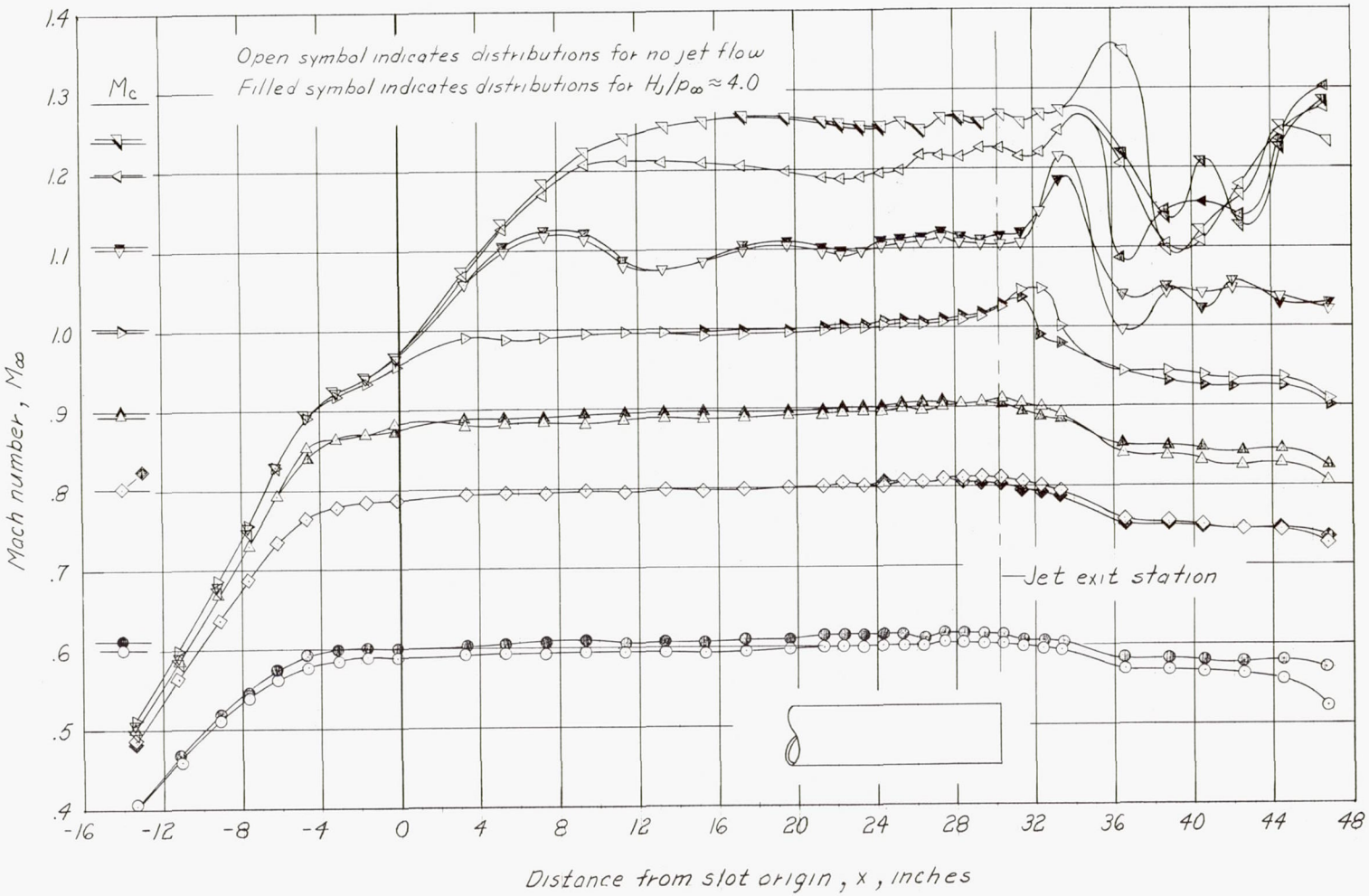

(b) Distributions for no jet flow and for $H_j/p_\infty \approx 4$.

Figure 5.- Concluded.

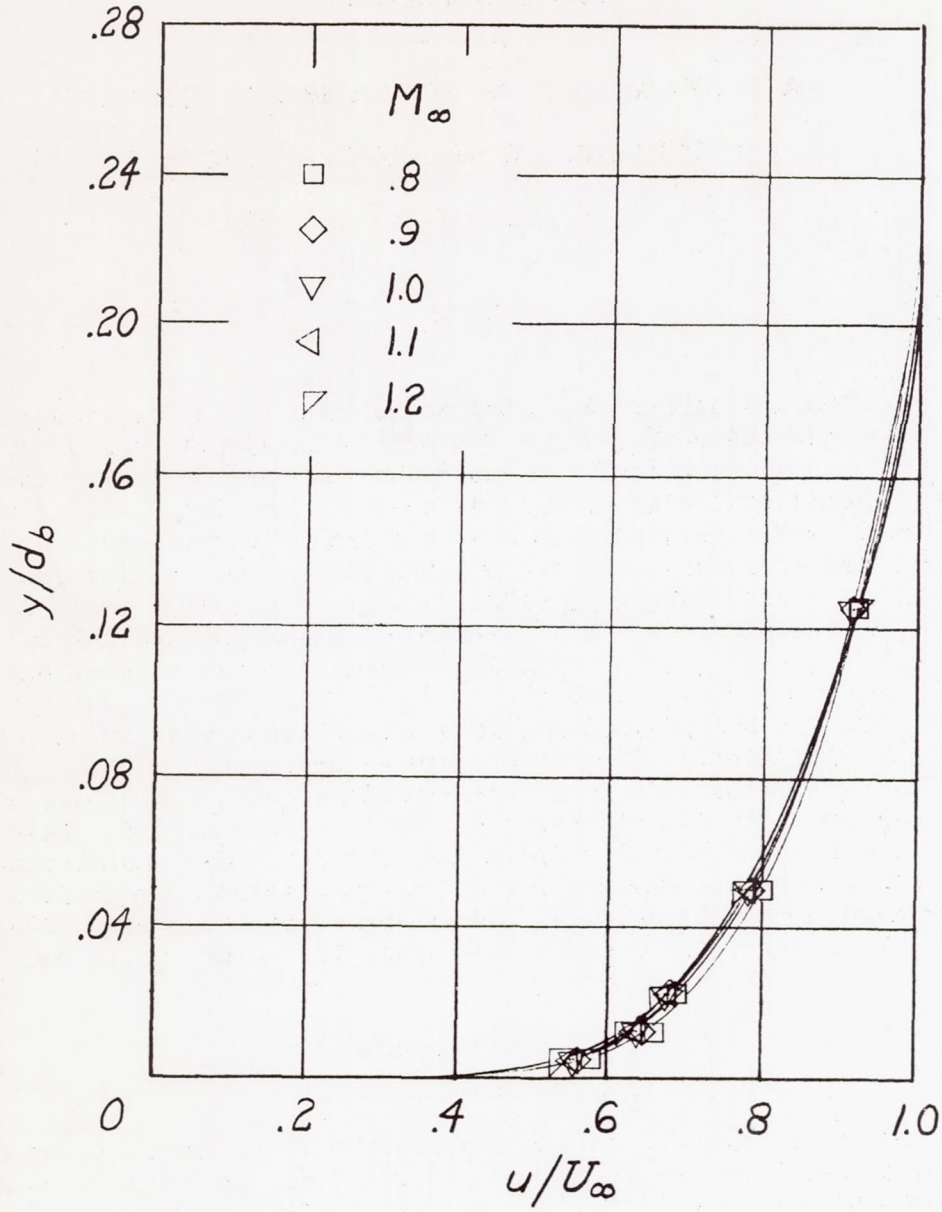

(a) Velocity profiles at several free-stream Mach numbers.

Figure 6.- Boundary-layer profiles $5\frac{1}{2}$ inches upstream from base of model.

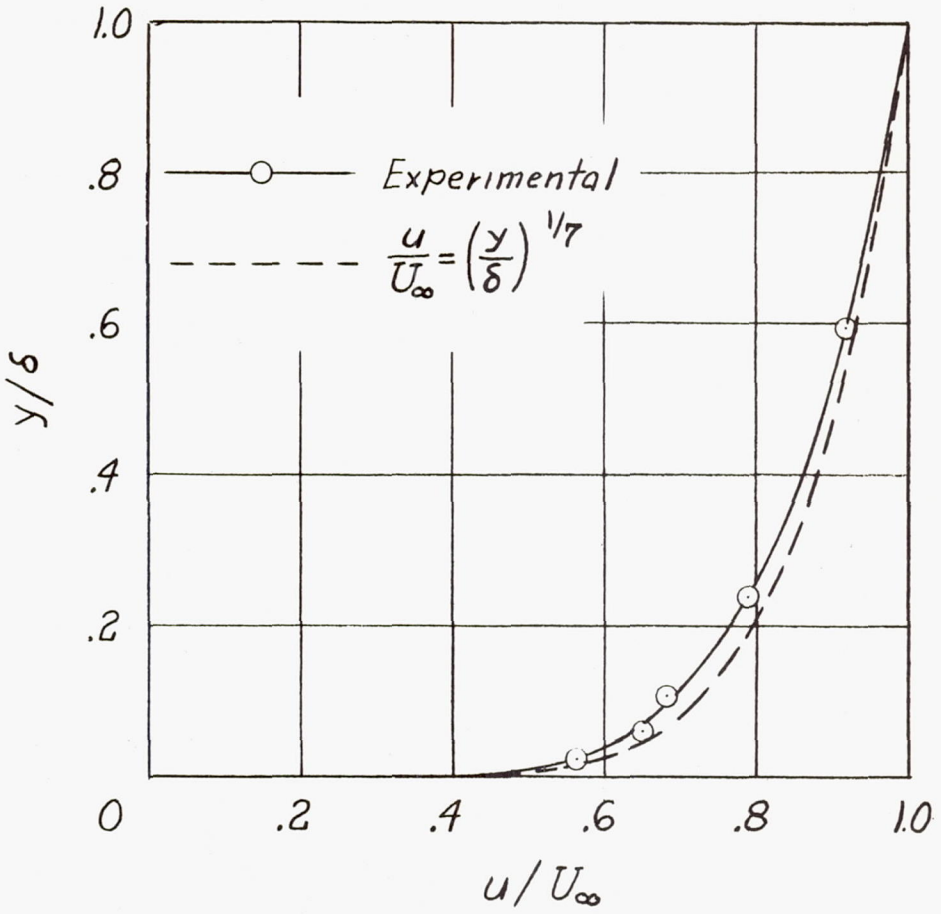

(b) Comparison of boundary-layer profile at $M_\infty = 0.9$ with 1/7-power profile.

Figure 6.- Concluded.

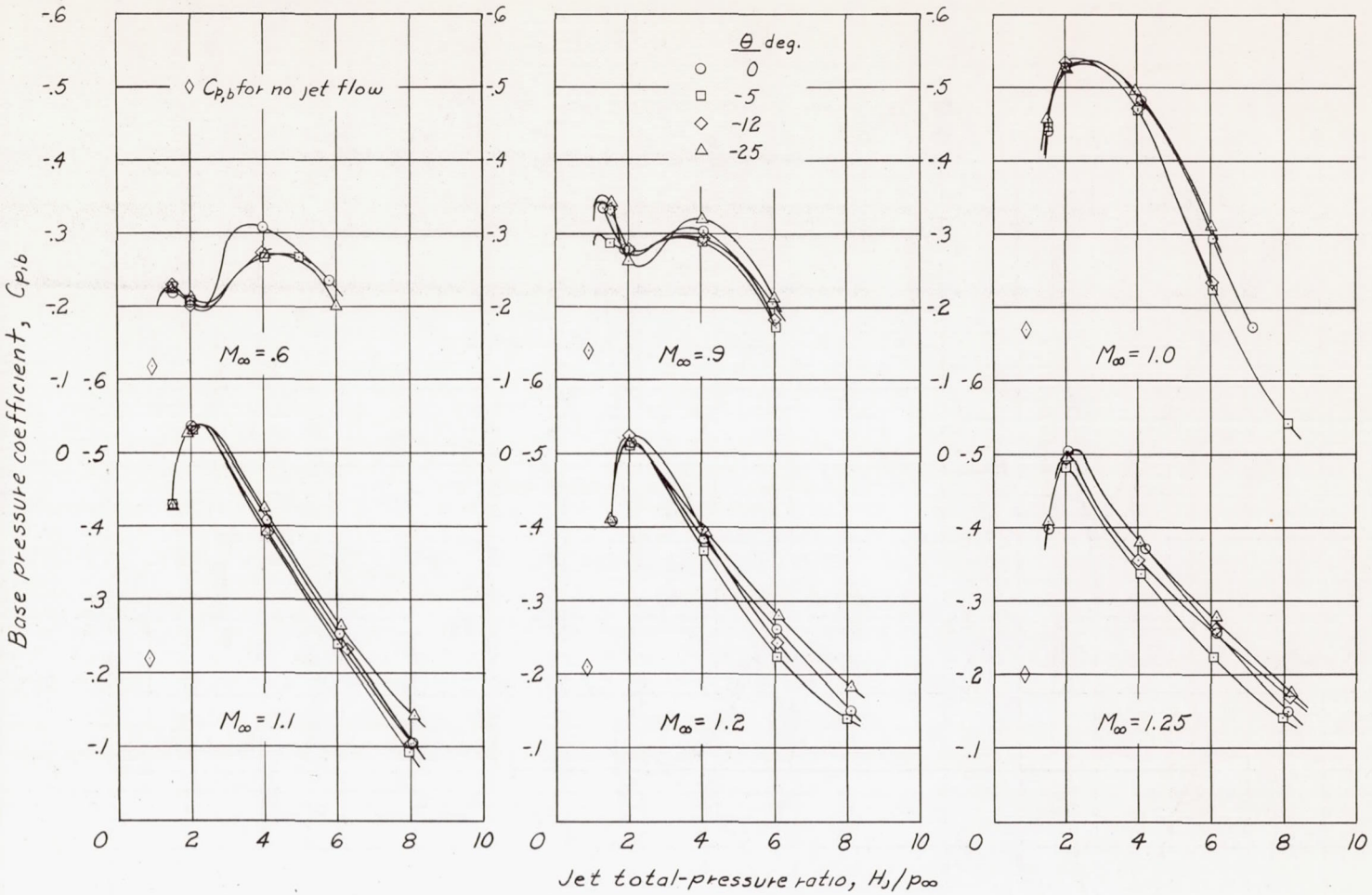

(a) $d_j/d_b = 0.65$.

Figure 7.- Effect of jet total-pressure ratio on base pressure coefficient; sonic nozzles.

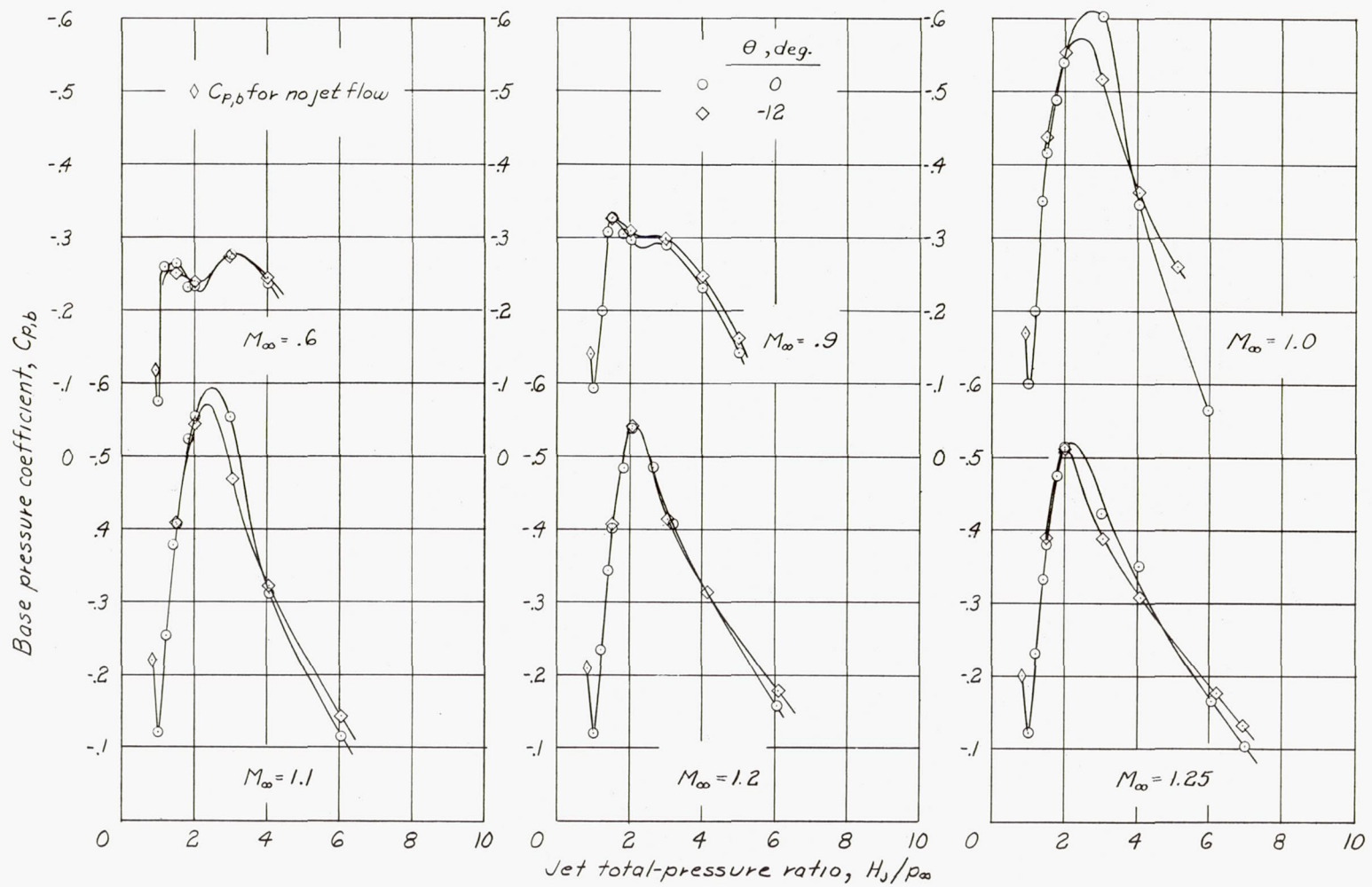

(b) $d_j/d_b = 0.75$.

Figure 7.- Continued.

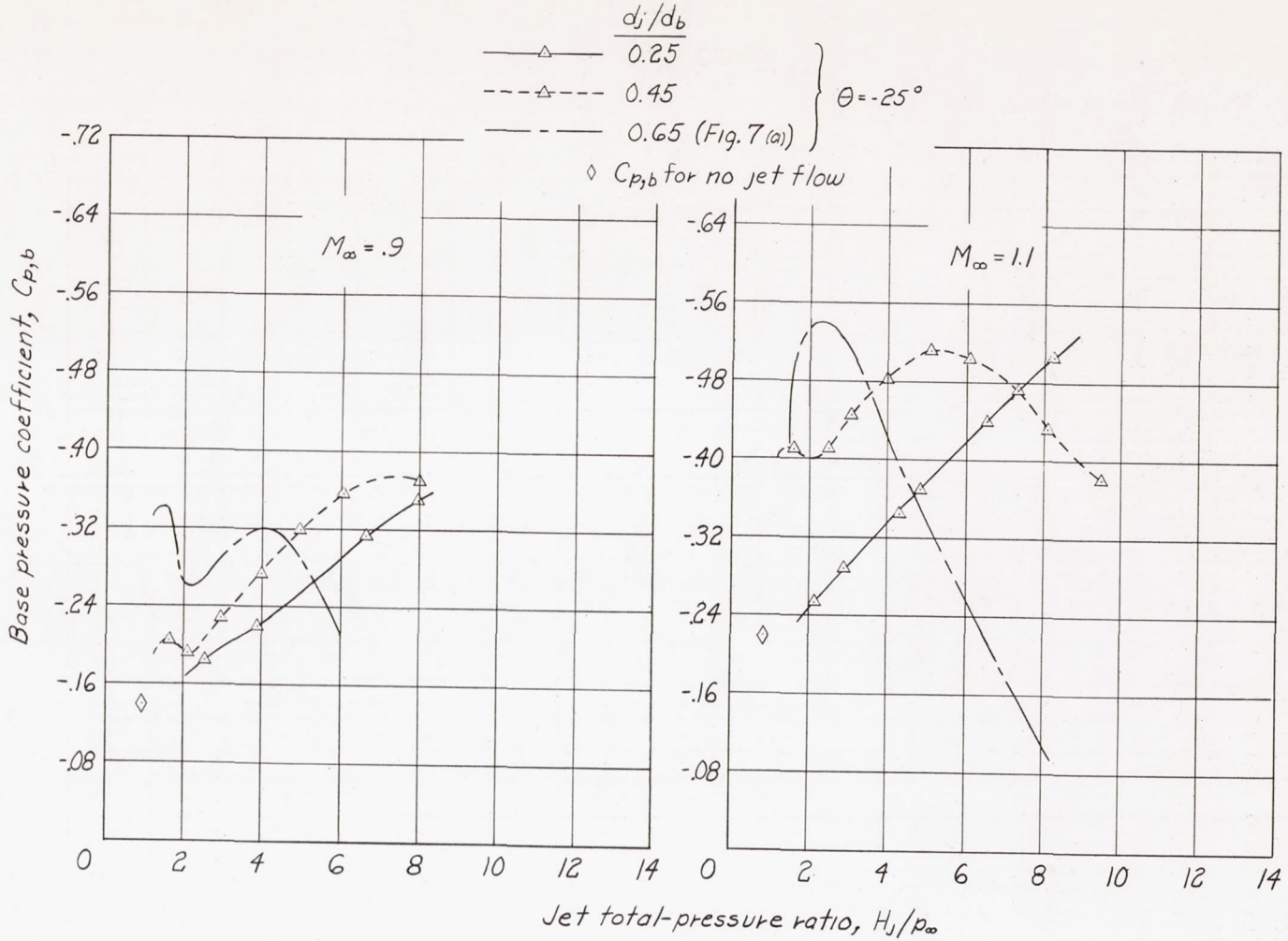

(c) d_j/d_b = 0.25 and 0.45.

Figure 7.- Concluded.

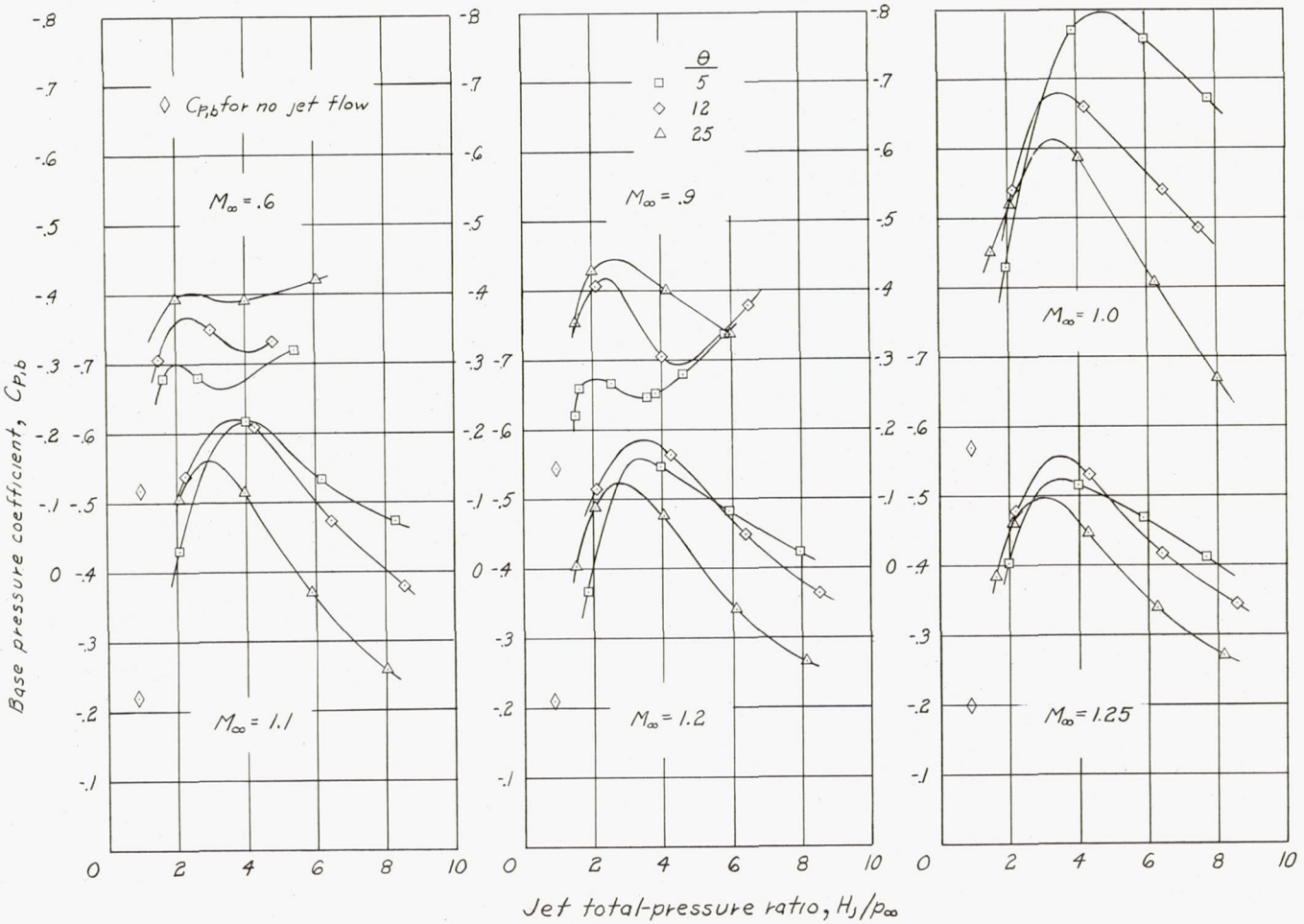

(a) $d_j/d_b = 0.75$.

Figure 8.- Effect of jet total-pressure ratio on base pressure coefficient; supersonic nozzles.

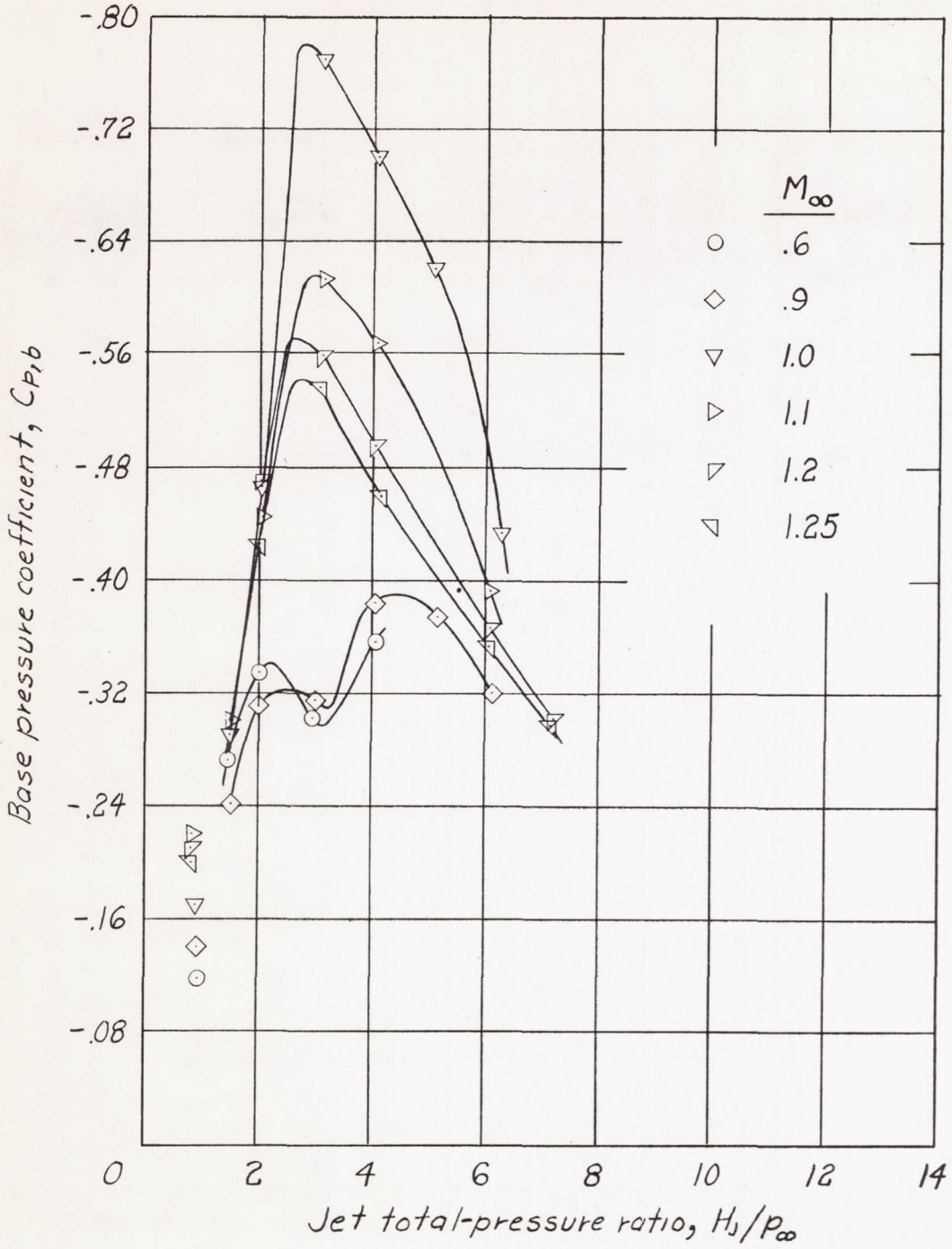

(b) $\theta = 12^\circ$; $d_j/d_b = 0.85$.

Figure 8.- Concluded.

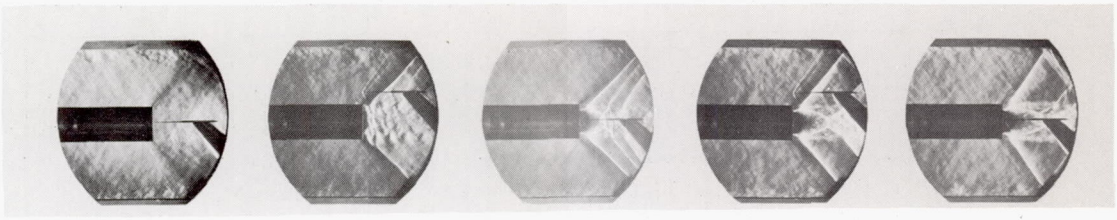

(a) (b) (c) (d) (e)

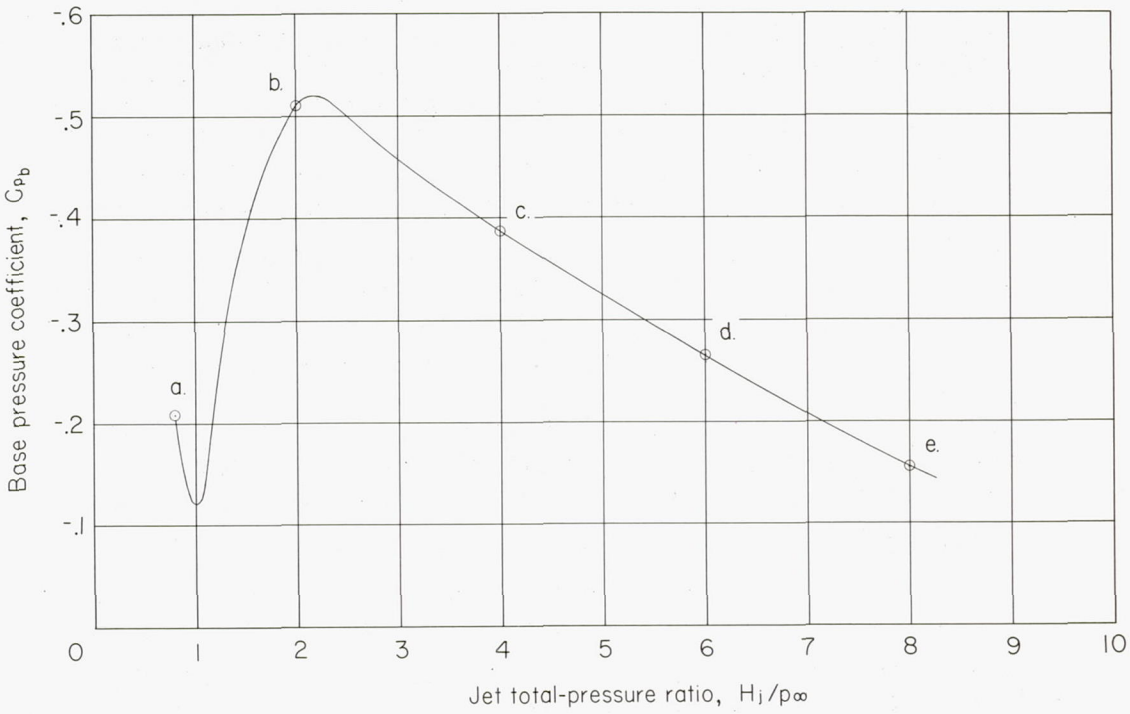

(a) $M_\infty = 1.20$.

Figure 9.- Typical variation of base pressure coefficient with jet total-pressure ratio, and schlieren photographs of the flow at several jet total-pressure ratios.

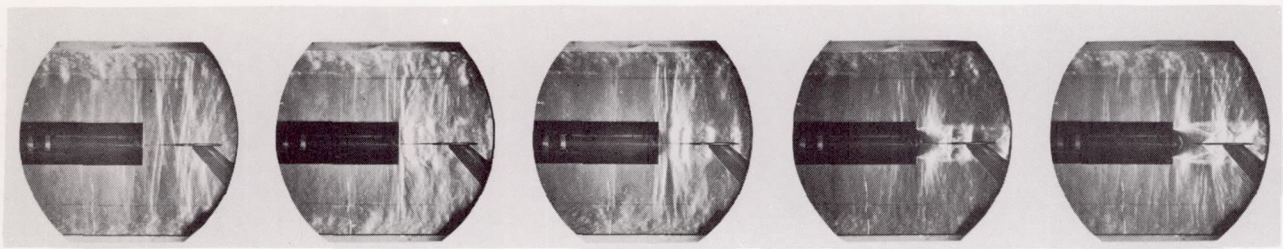

(a) (b) (c) (d) (e)

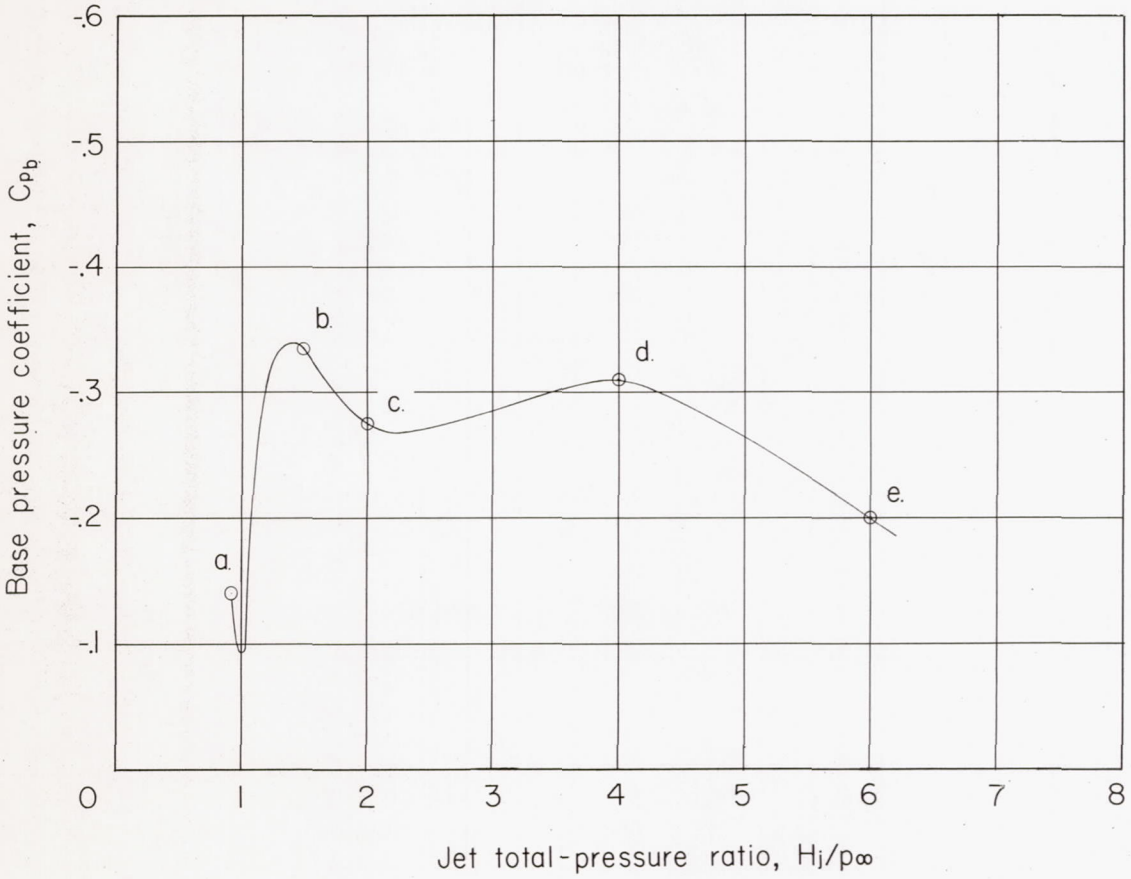

(b) $M_\infty = 0.9$.

Figure 9.- Concluded.

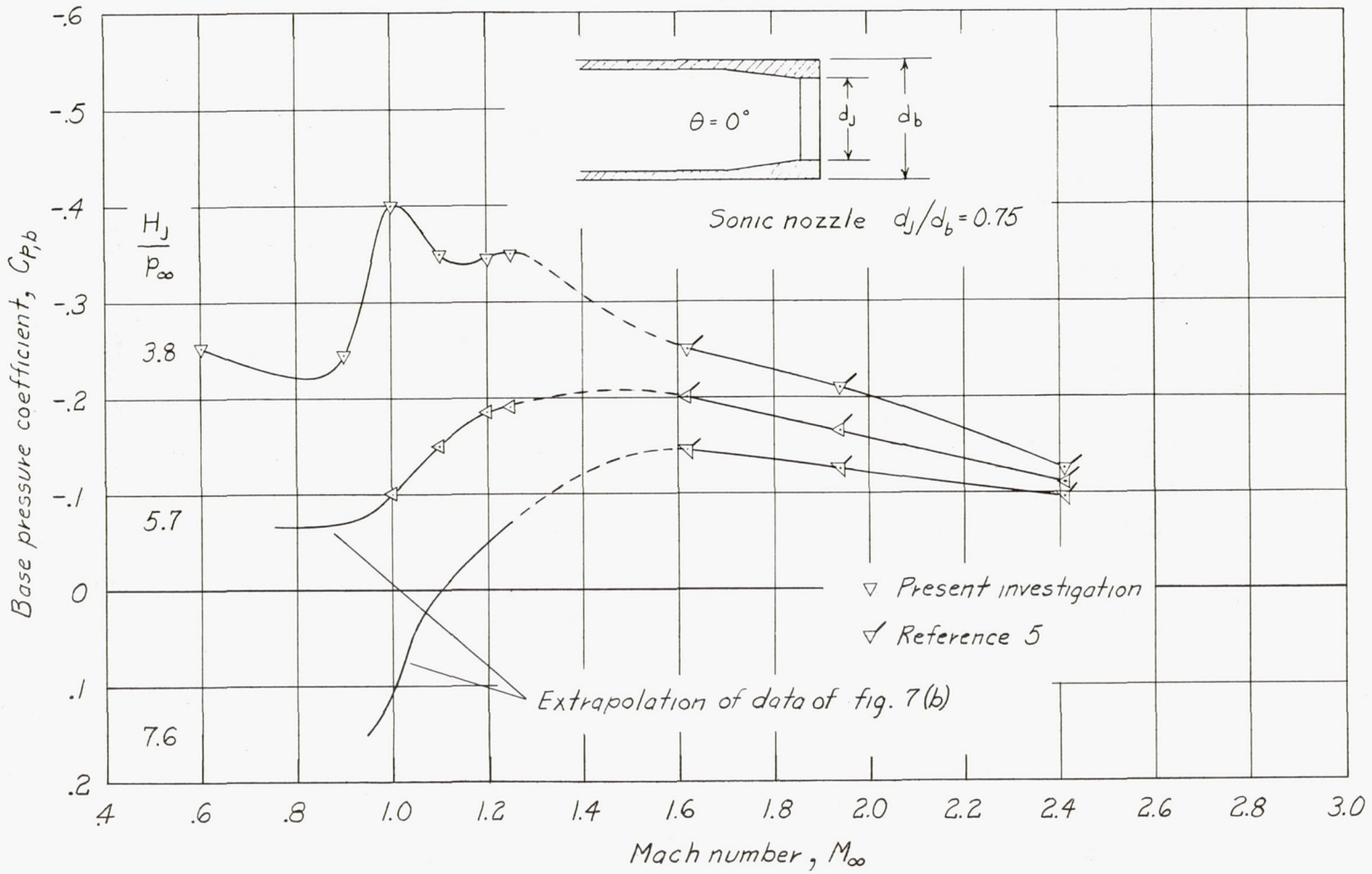

(a) Sonic nozzle.

Figure 10.- Extension of present data by use of data from reference 5.

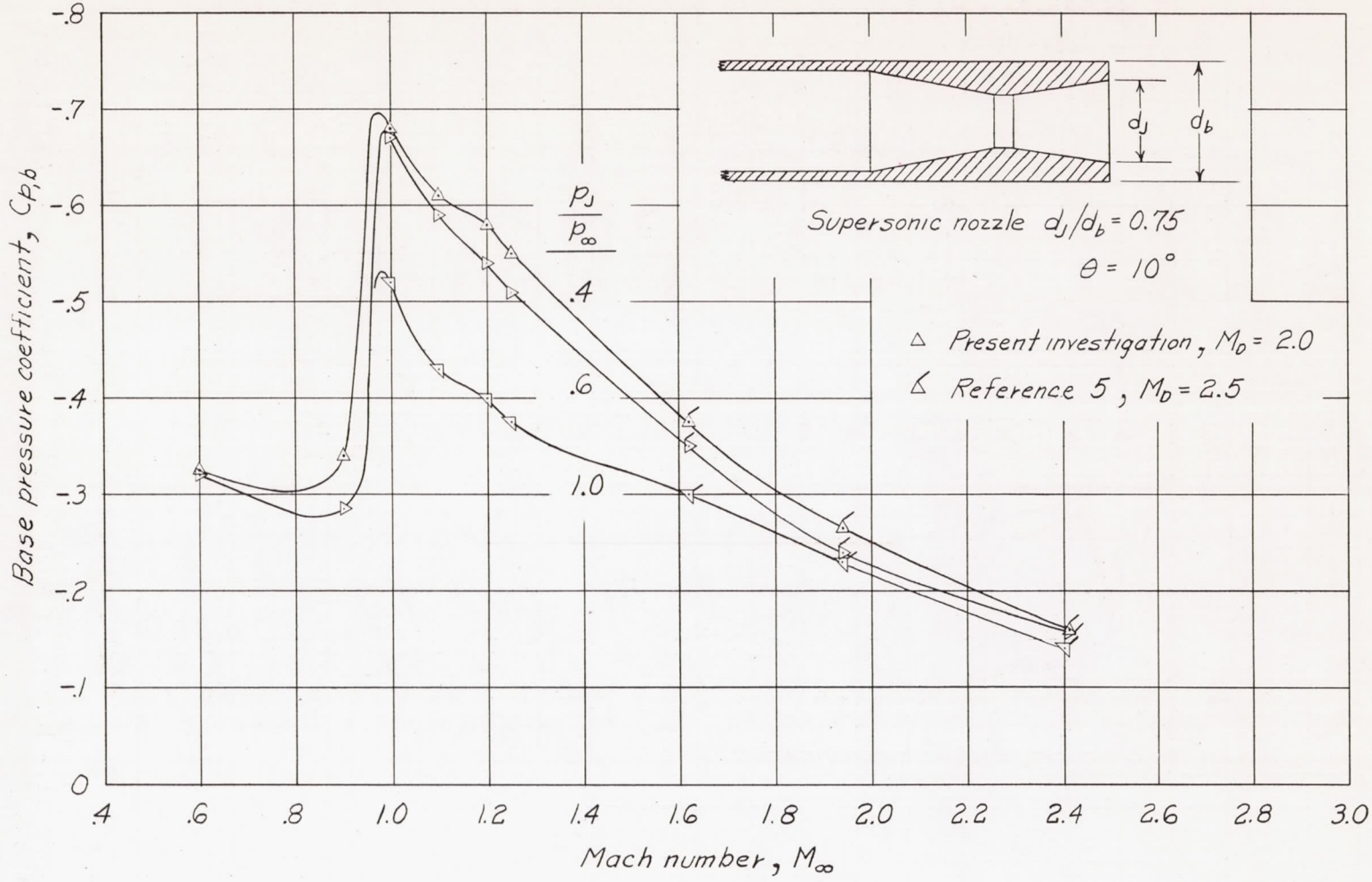

(b) Supersonic nozzle.

Figure 10.- Concluded.

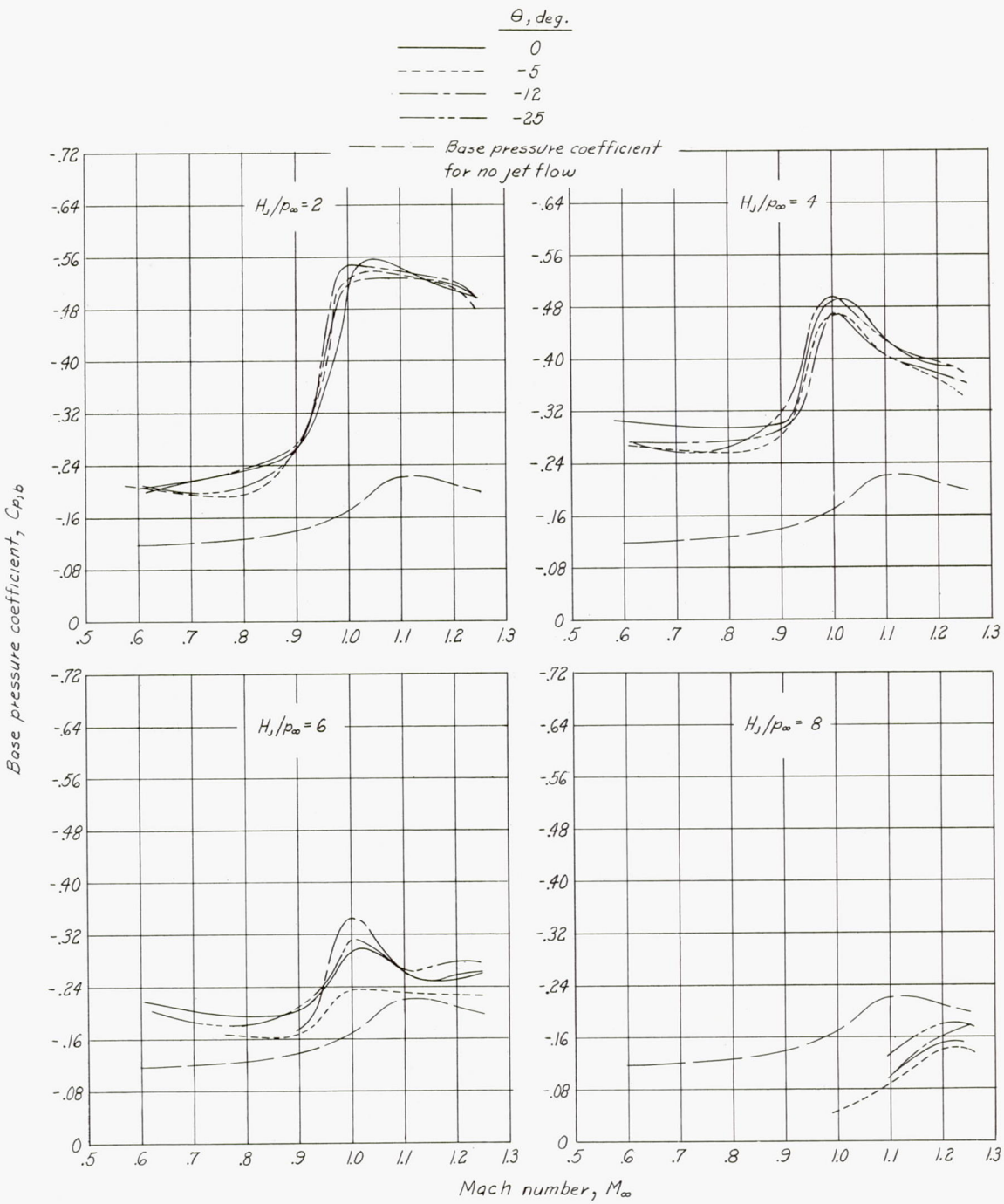

(a) Sonic nozzle; $d_j/d_b = 0.65$.

Figure 11.- Effect of Mach number on base pressure coefficient.

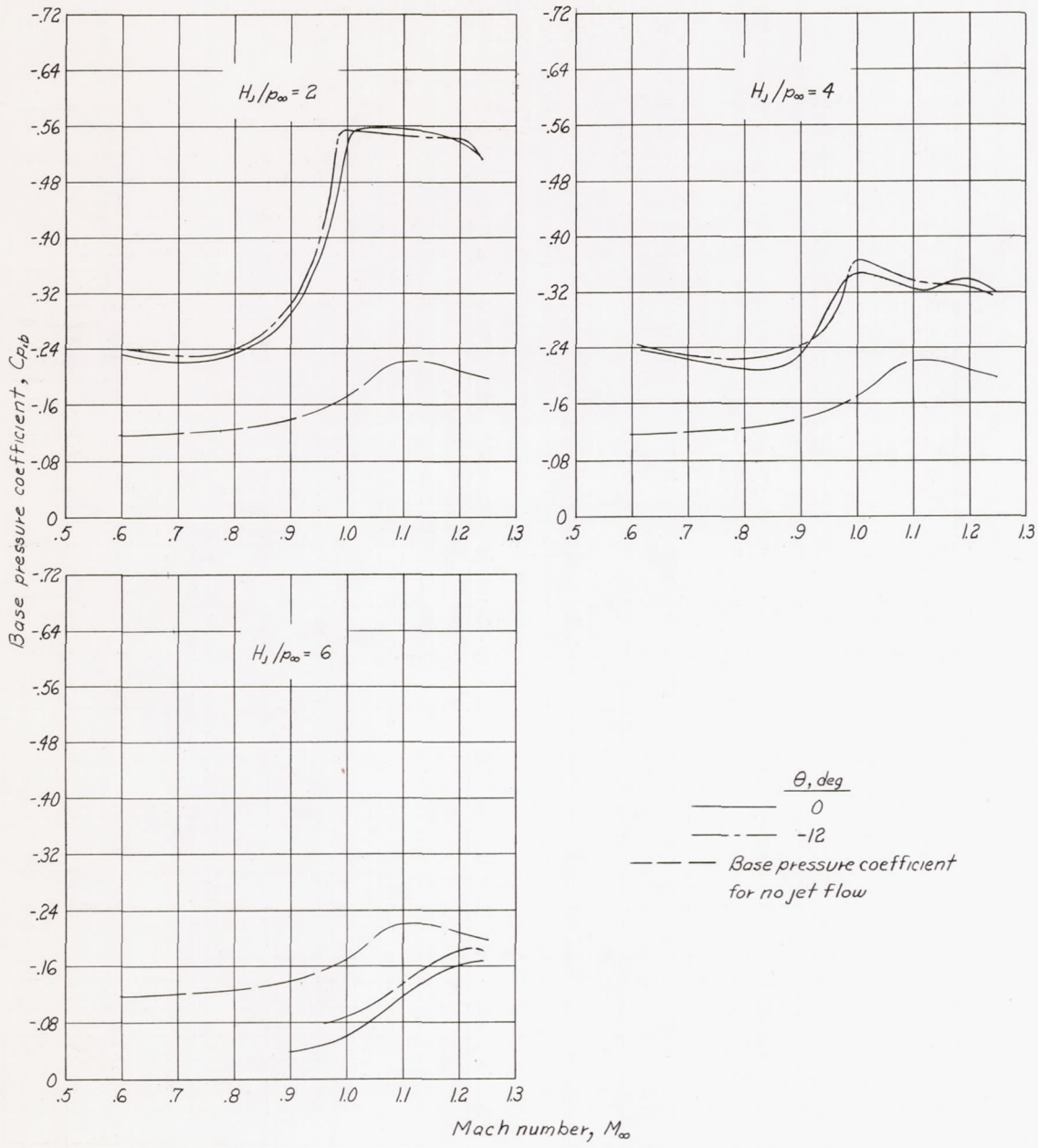

(b) Sonic nozzle; $d_j/d_b = 0.75$.

Figure 11.- Continued.

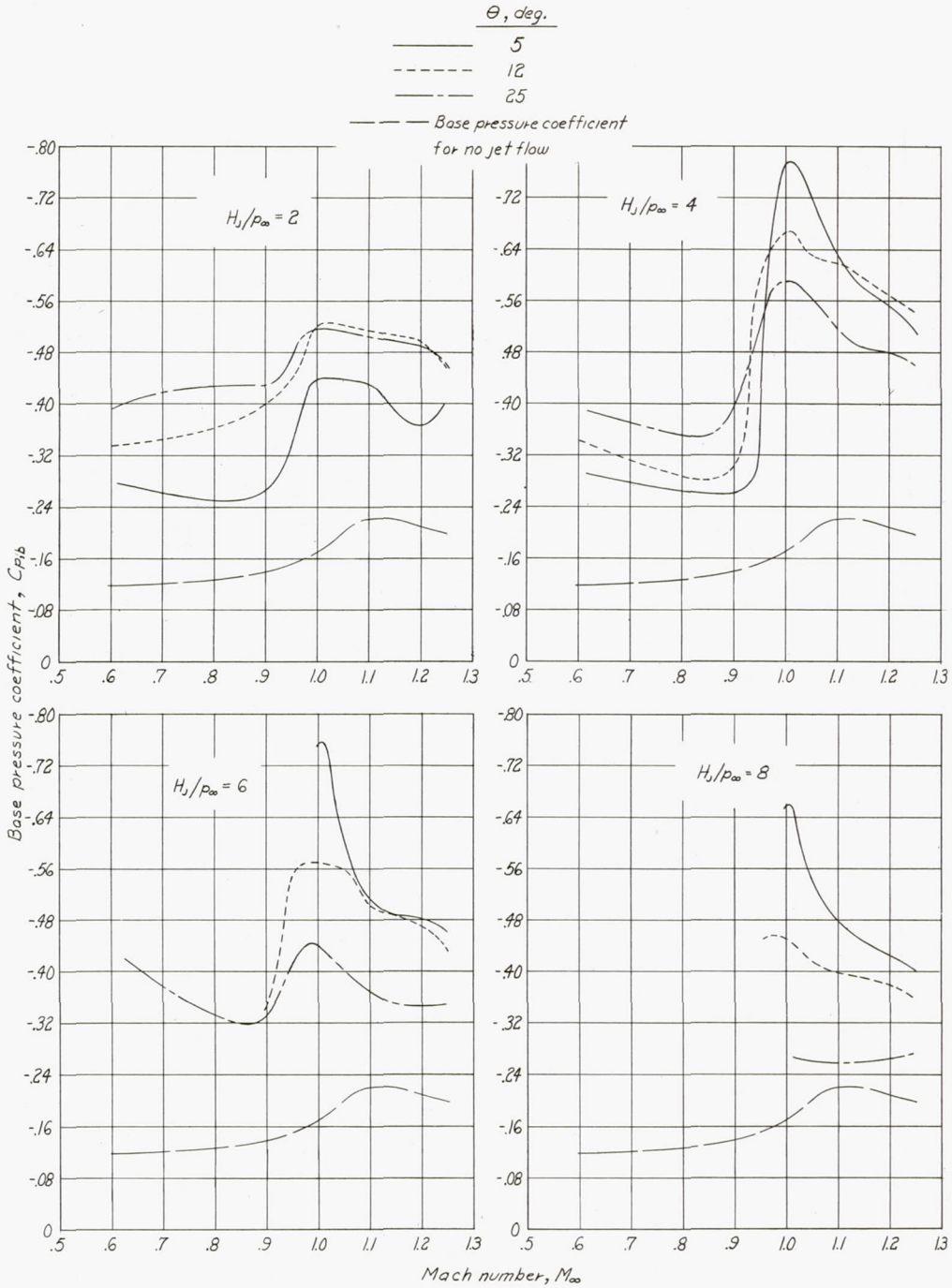

(c) Supersonic nozzle; $d_j/d_b = 0.75$.

Figure 11.- Continued.

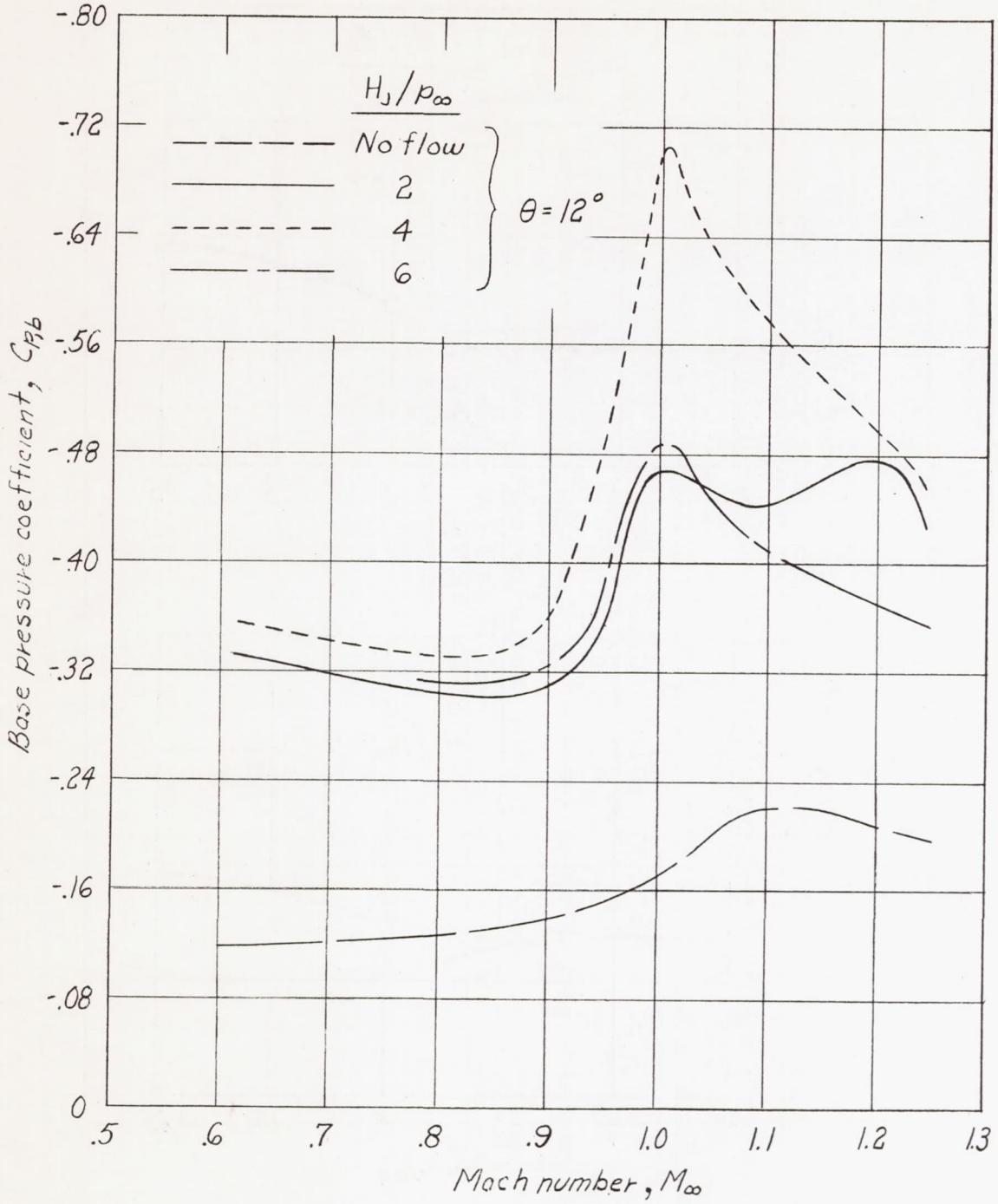

(d) Supersonic nozzle; $d_j/d_b = 0.85$.

Figure 11.- Concluded.

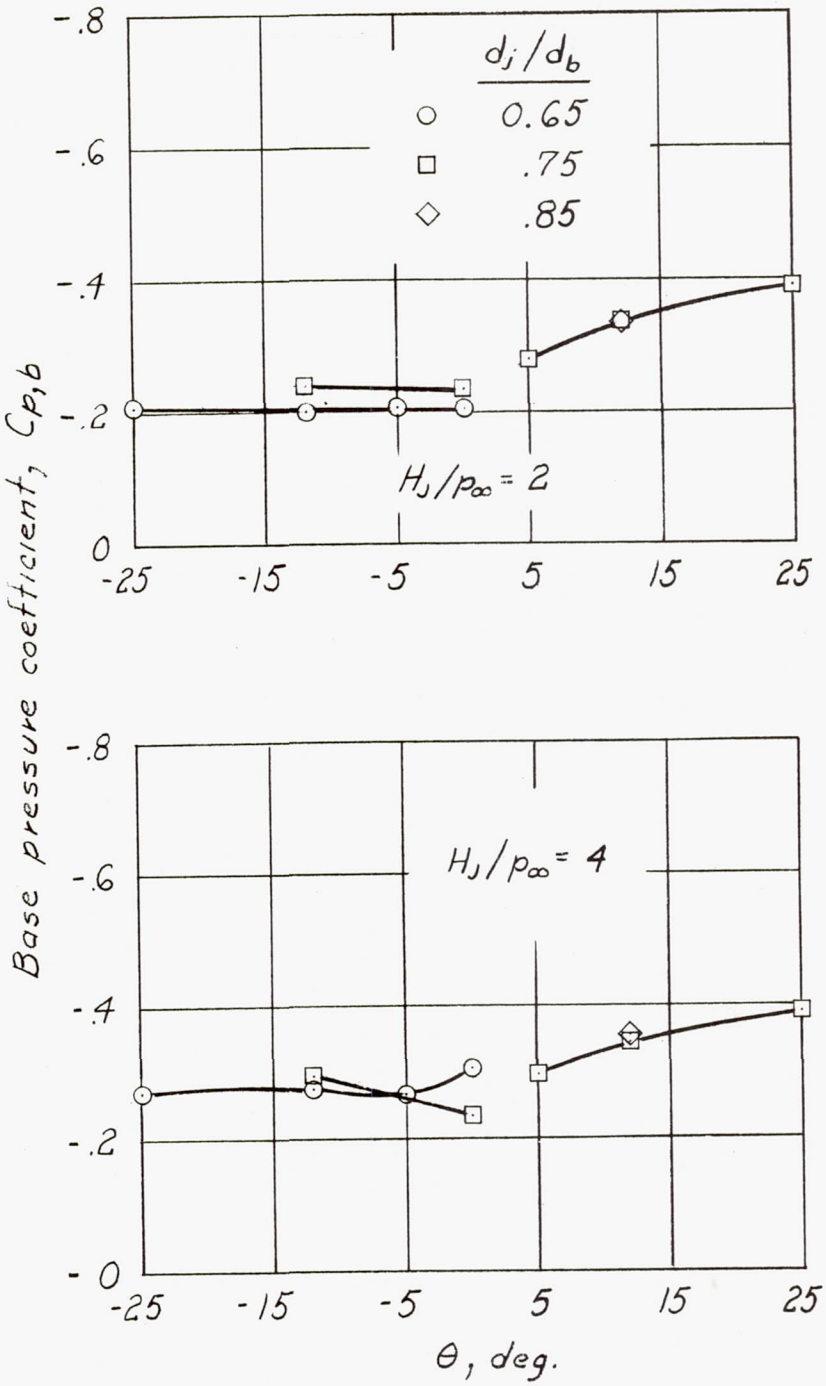

(a) $M_\infty = 0.6$.

Figure 12.- Effect of nozzle geometry on base pressure coefficient.

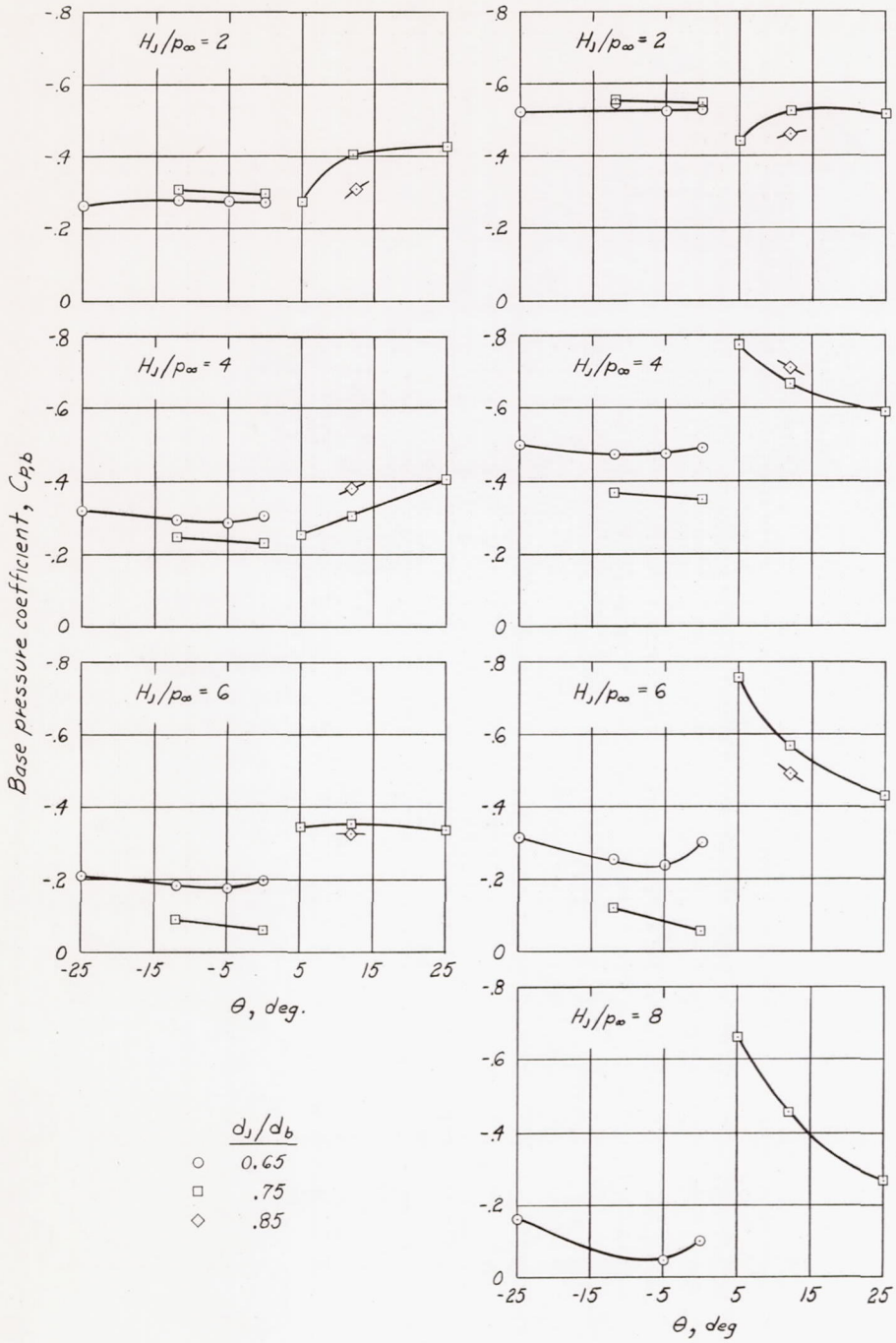

(b) $M_\infty = 0.9$. (c) $M_\infty = 1.0$.

Figure 12.- Continued.

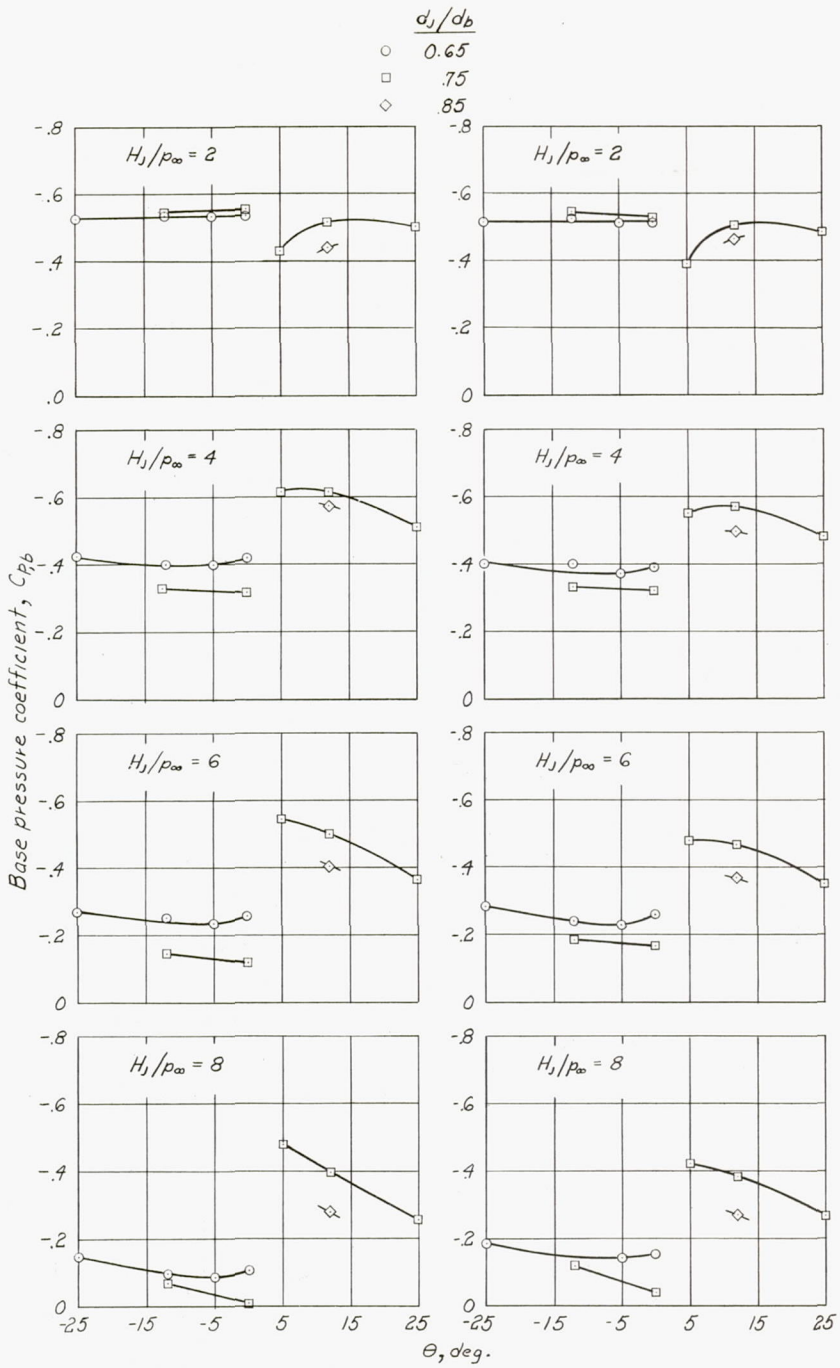

(d) $M_\infty = 1.1$. (e) $M_\infty = 1.2$.

Figure 12.- Concluded.

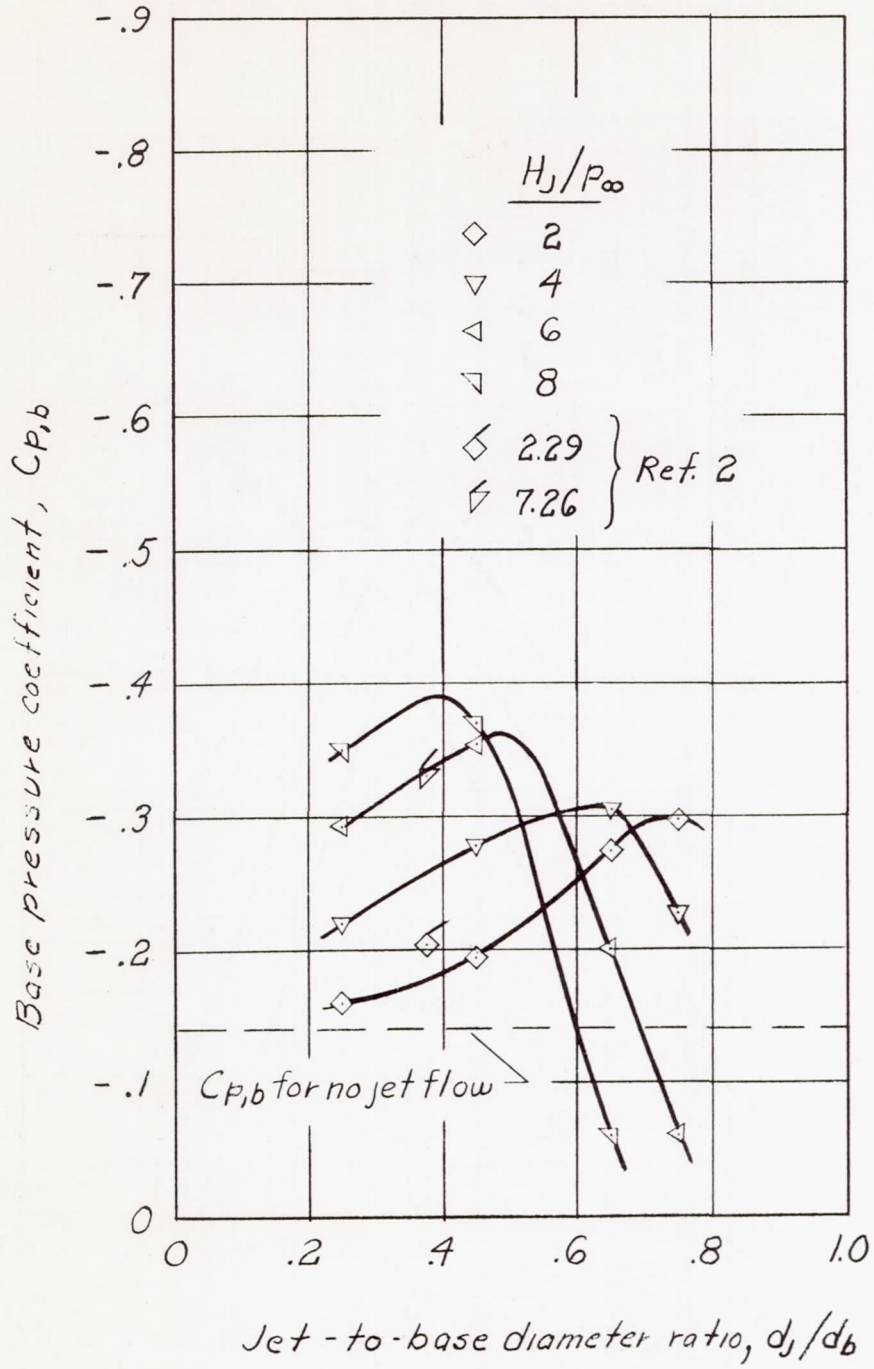

(a) $M_\infty = 0.9$.

Figure 13.- Effect of jet-to-base diameter ratio on base pressure coefficient for the sonic nozzle.

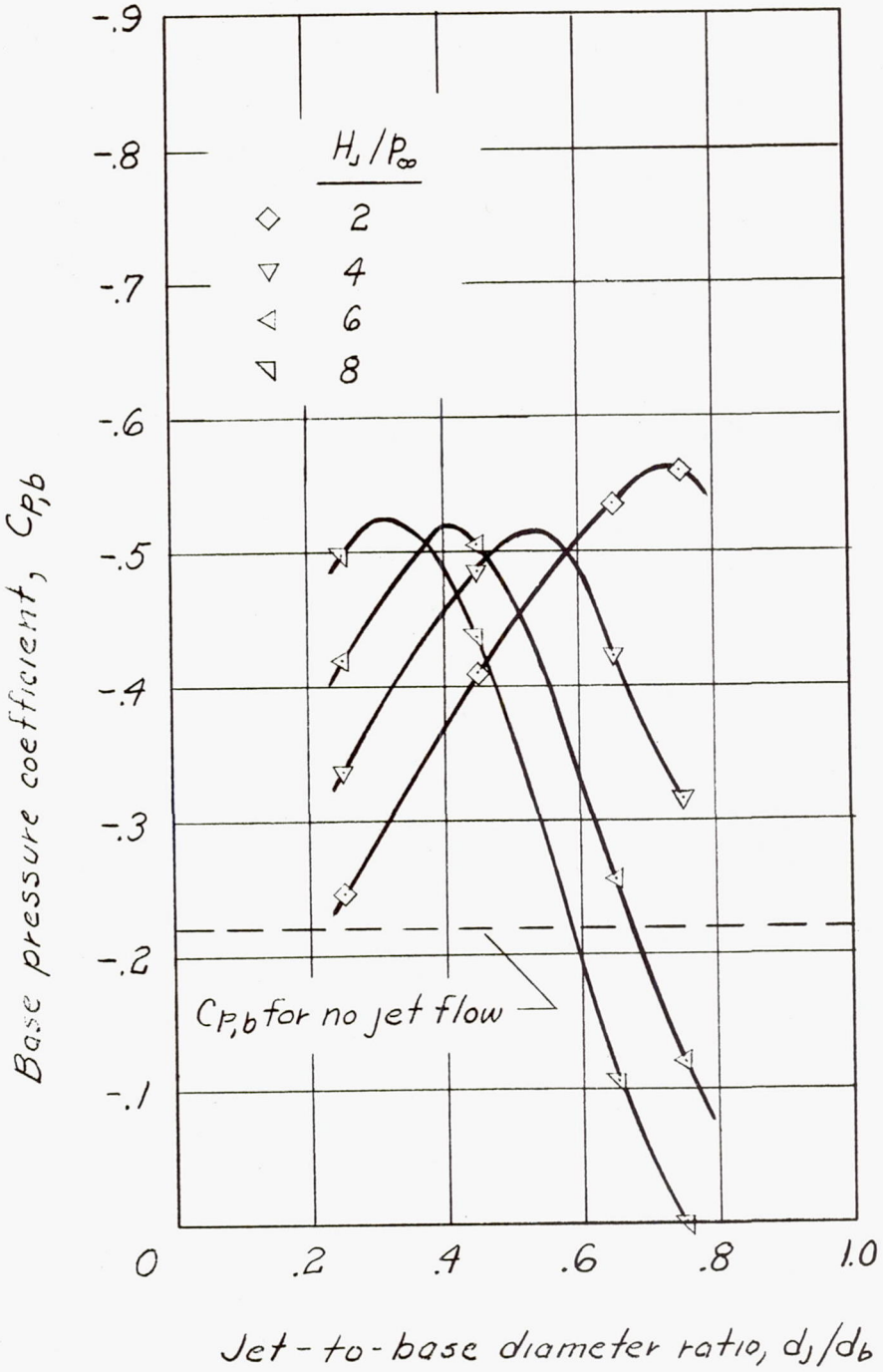

(b) $M_\infty = 1.10$.

Figure 13.- Concluded.

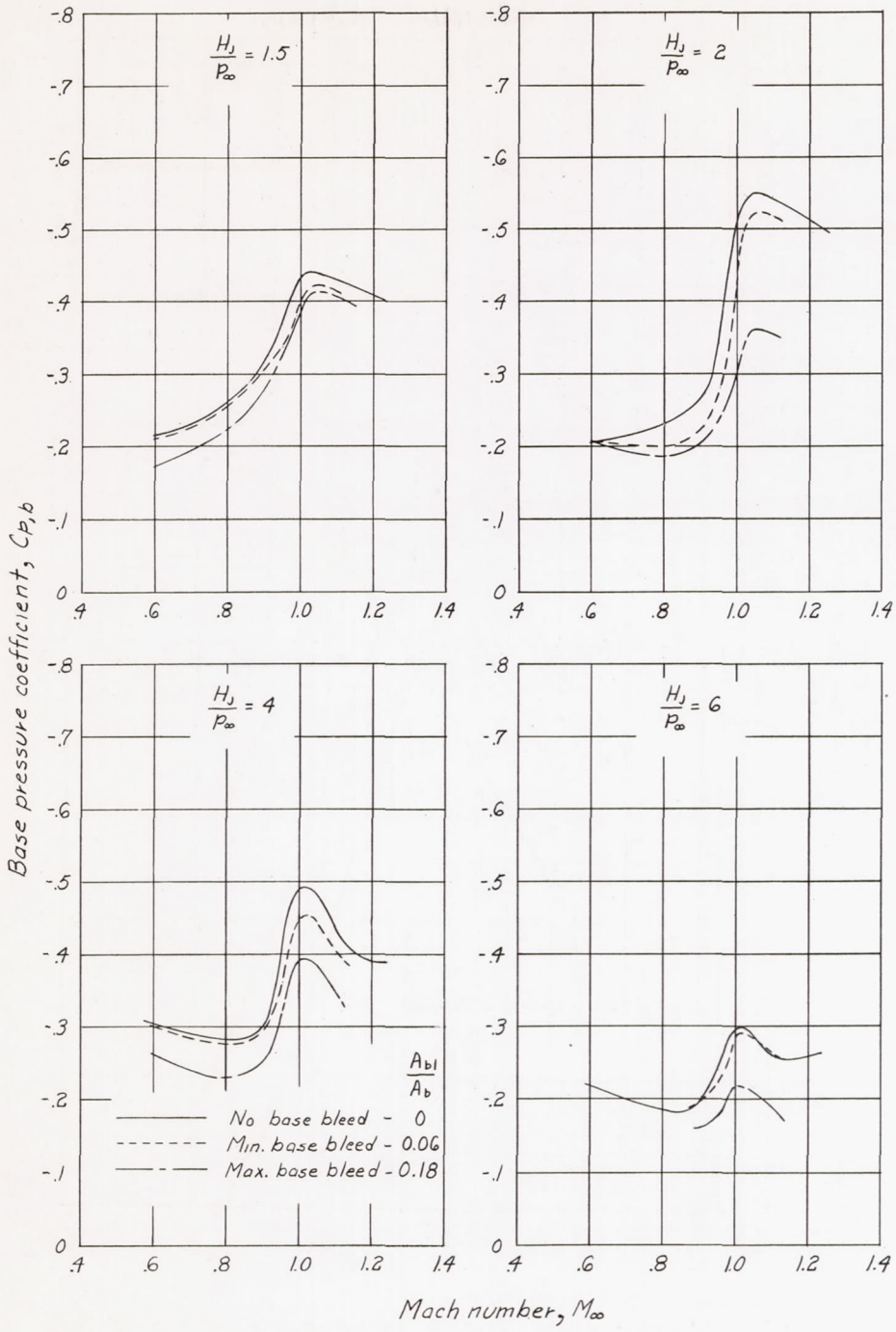

(a) $\theta = 0^\circ$; $d_j/d_b = 0.65$.

Figure 14.- Effect of base bleed on base pressure coefficient at several jet total-pressure ratios.

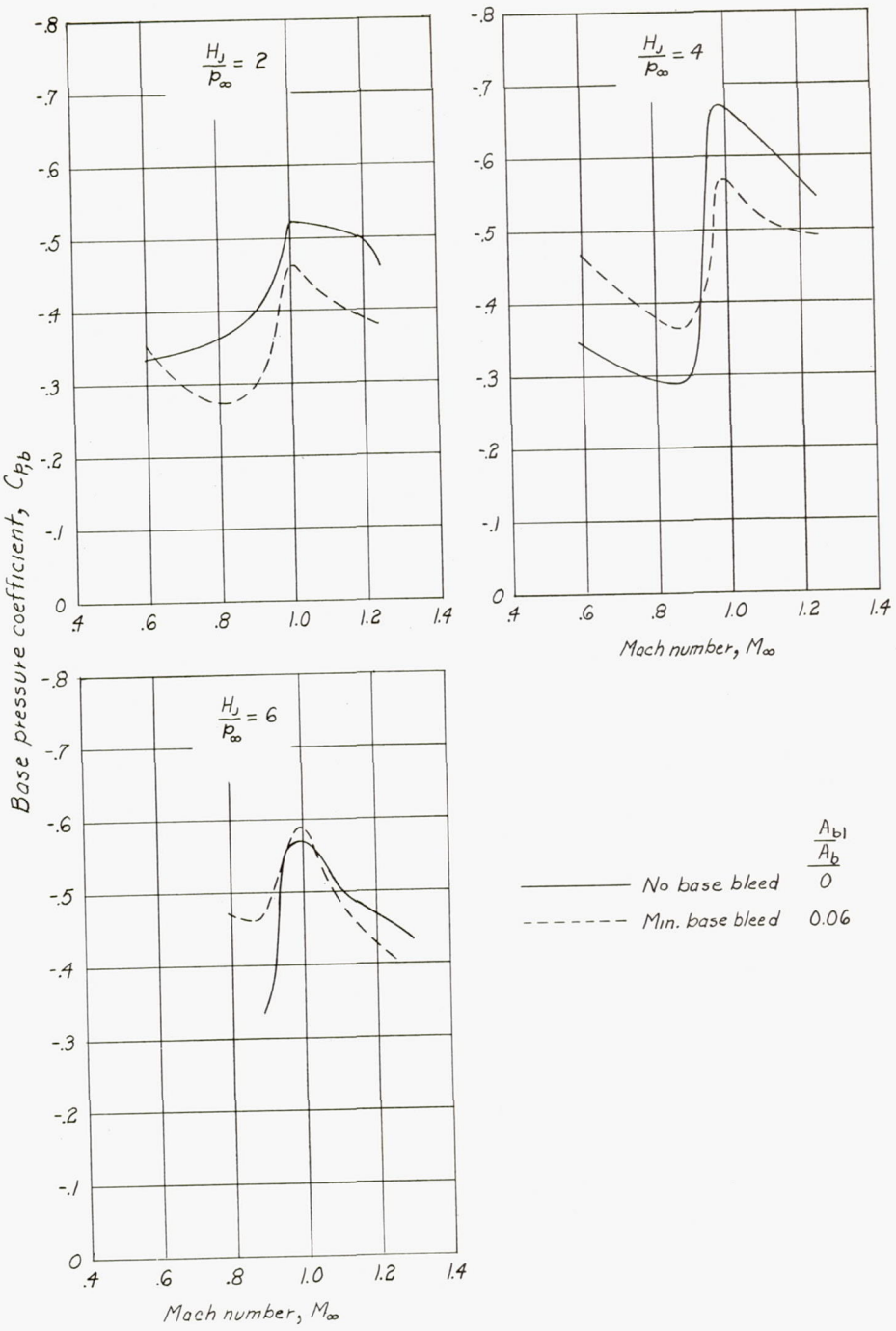

(b) $\theta = 12^\circ$; $d_j/d_b = 0.75$.

Figure 14.- Concluded.

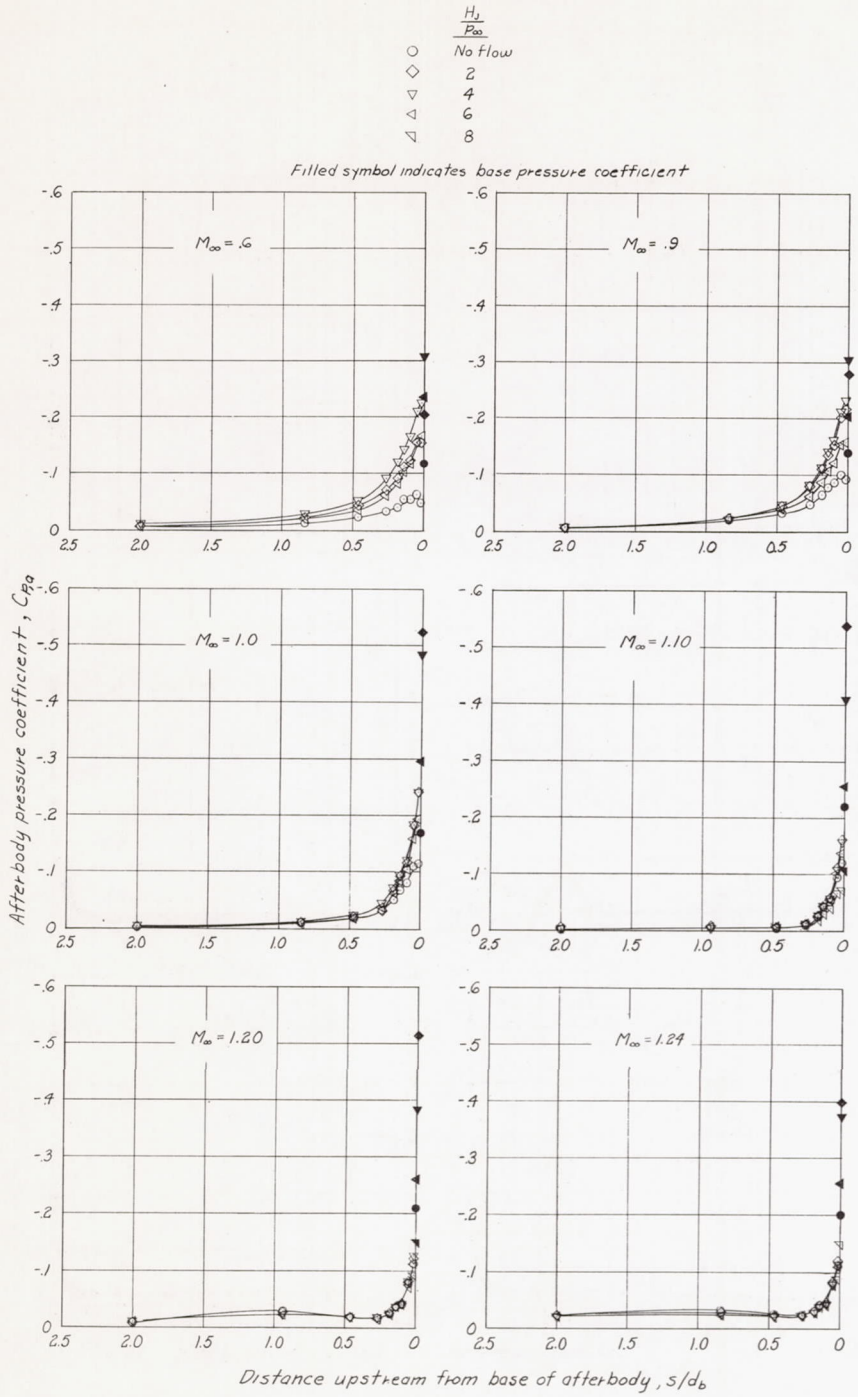

(a) $\theta = 0^\circ$; $d_j/d_b = 0.65$.

Figure 15.- Afterbody pressure distributions.

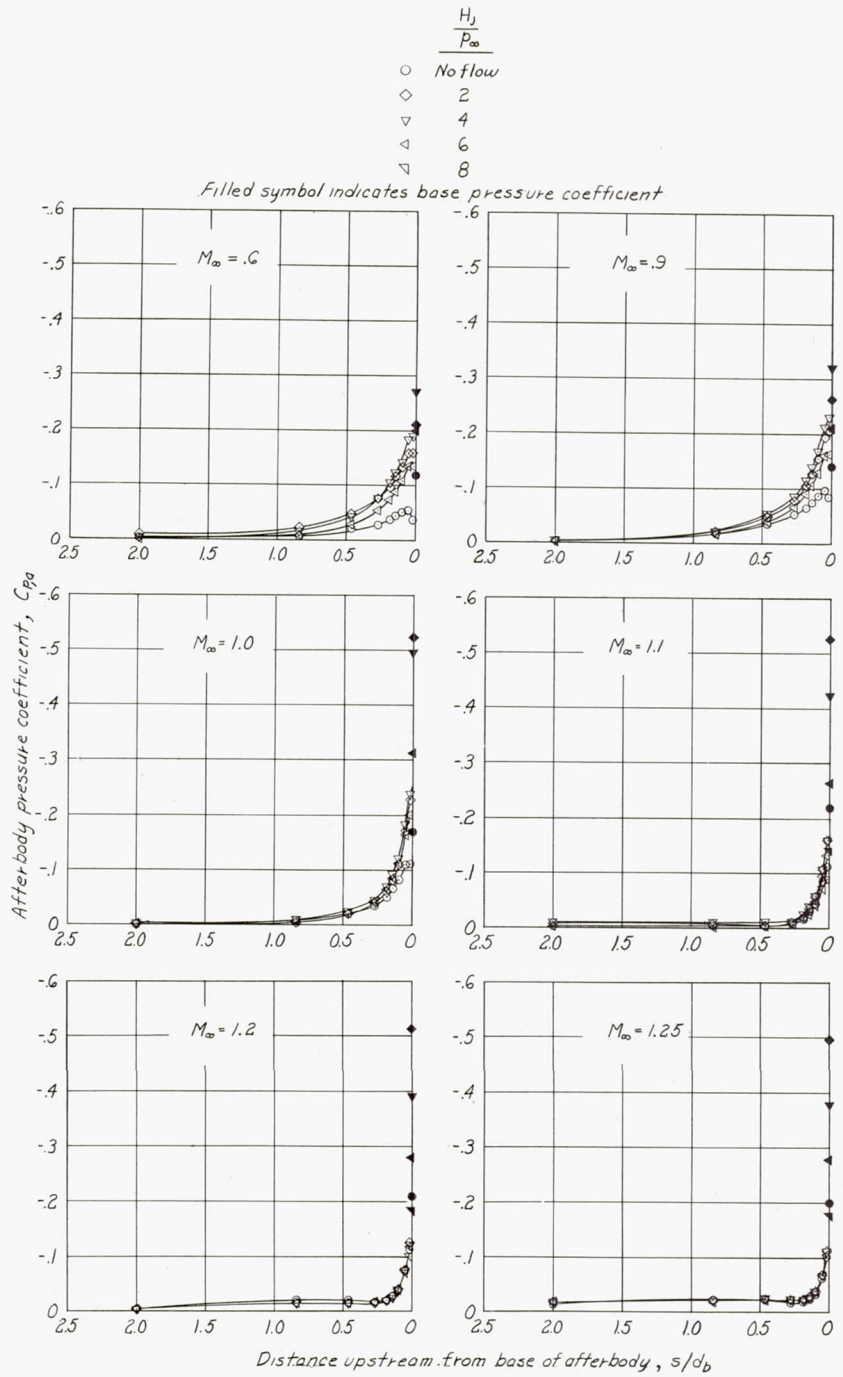

(b) $\theta = -25^\circ$; $d_j/d_b = 0.65$.

Figure 15.- Continued.

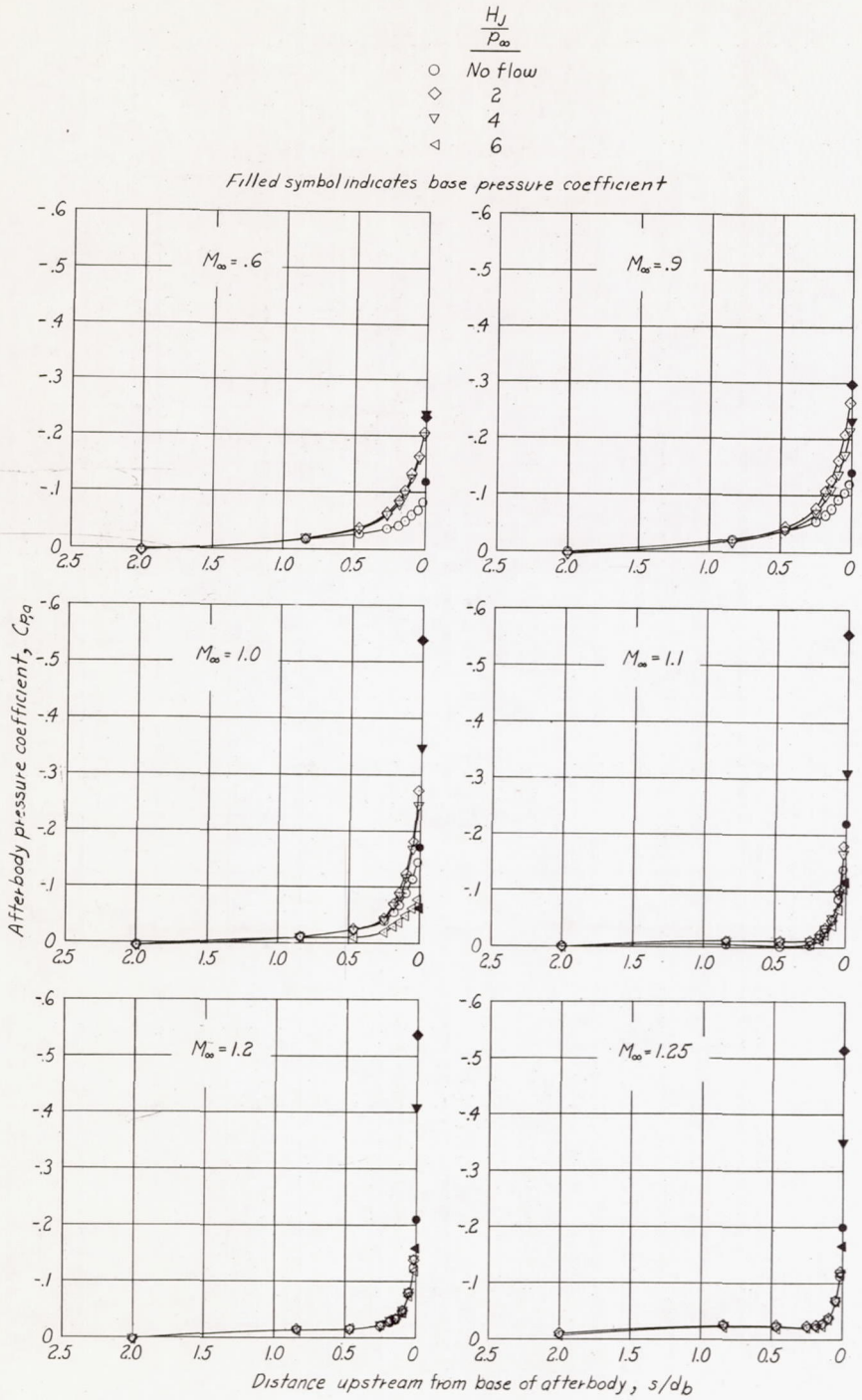

(c) $\theta = 0^\circ$; $d_j/d_b = 0.75$.

Figure 15.- Continued.

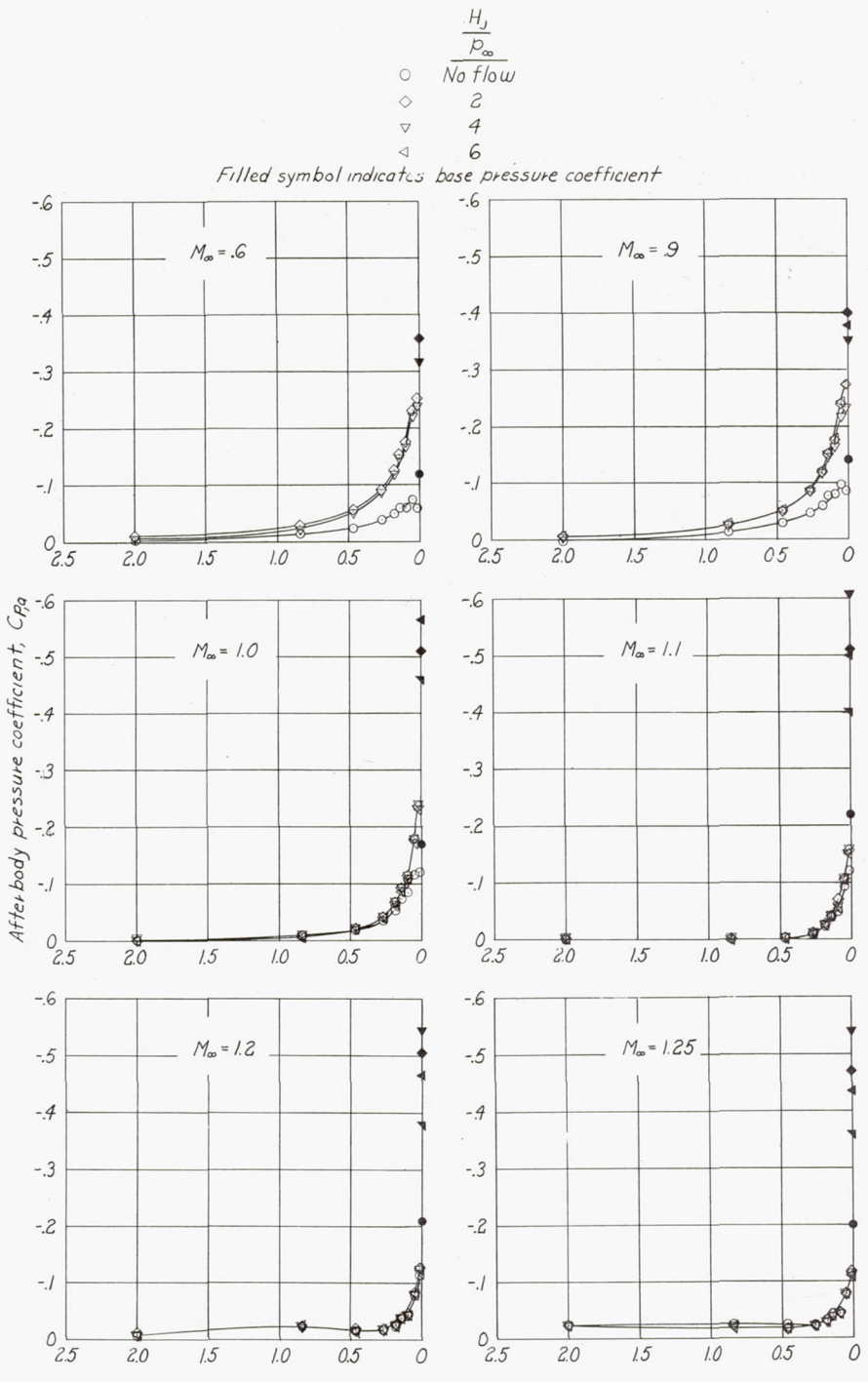

(d) $\theta = 12^\circ$; $d_j/d_b = 0.75$.

Figure 15.- Concluded.